Atmospheric
Chemistry
and Physics
Discussions

1   Tropospheric Ozone Seasonal and Long-term Variability as seen by lidar and

2   surface measurements at the JPL-Table Mountain Facility, California

3   Maria Jose Granados-Muñoz[1] and Thierry Leblanc[1]

4   1 Jet Propulsion Laboratory, California Institute of Technology, Wrightwood, CA, USA

5

6

7

8

9

10

11

12

13

14

15

16

17

18

19

20   Corresponding author: mamunoz@jpl.nasa.gov

Atmospheric
Chemistry
and Physics
Discussions

23

Abstract

25 A combined surface and tropospheric ozone climatology and interannual variability study

26 was performed for the first time using co-located ozone photometer measurements (2013-2015)

27 and tropospheric ozone differential absorption lidar measurements (2000-2015) at the Jet

28 Propulsion Laboratory Table Mountain Facility (TMF, elev. 2285 m), in California.

29 The surface time-series were investigated both in terms of seasonal and diurnal variability.

30 The observed surface ozone is typical of high-elevation remote-sites, with small amplitude of the

31 seasonal and diurnal cycles, and high ozone values, compared to neighboring lower altitude

32 stations representative of urban boundary layer conditions. The ozone mixing ratio ranges from

33 45 ppbv in the winter morning hours to 65 ppbv in the spring and summer afternoon hours. At

34 the time of the lidar measurements (early night), the seasonal cycle observed at the surface is

35 similar to that observed by lidar between 3.5 km and 9 km.

36 Above 9 km, the local tropopause height variation with time and season impacts significantly

37 the ozone lidar observations. The frequent tropopause folds found in the vicinity of TMF (27%

38 of the time, mostly in winter and spring) produce a dual vertical structure in ozone within the

39 fold layer, characterized by higher-than-average values in the bottom half of the fold (12-14 km),

40 and lower-than-averaged values in the top half of the fold (14-18 km). This structure is consistent

41 with the expected origin of the air parcels within the fold, i.e., mid-latitude stratospheric air

42 folding down below the upper tropospheric sub-tropical air.

43 No significant signature of interannual variability could be observed on the 2000-2015

44 deseasonalized lidar time-series, with only a statistically non-significant positive anomaly during

45 the years 2003-2007. Our trend analysis reveals however a statistically significant positive trend

46 of 0.31 ppbv.year^{-1} in the free troposphere for the period 2000-2015.

47 A classification of the air parcels sampled by lidar was made at 1-km interval between 5 km

48 and 14 km altitude, using 8-days backward trajectories (HYSPLIT). Our classification revealed

49 the large influence of the Pacific Ocean, with air parcels of low ozone content (50-65 ppbv), and

50 significant influence of the stratosphere leading to ozone values of 65-80 ppbv down to 8-9 km.

51   In summer, enhanced ozone values (70 ppbv) were found in air parcels originating from Central

52   America, probably owed to the enhanced thunderstorm activity during the North American

53   Monsoon. No outstanding influence from Asia was identified.

54

Atmospheric
Chemistry
and Physics
Discussions

Open Access

EGU

1. Introduction

Ozone is an important constituent in the troposphere, impacting climate, chemistry, and air quality (The Royal Society, 2008). As a greenhouse gas (Forster et al., 2007), it contributes to the Earth's global warming with an estimate radiative forcing of 0.40 ± 0.20 W·m^{-2} (IPCC 2013). It is one of the main oxidants in the troposphere (Monks, 2005), and, in high concentrations, it can cause problems in human health and vegetation (World Health Organization, 2003). Tropospheric ozone can be directly emitted to the troposphere, but it is primarily formed as a secondary pollutant in chemicals reactions involving ozone precursors such as methane, CO, NOx, VOCs or PANs. An additional source of ozone in the troposphere is the downward transport from the stratosphere, where ozone is much more abundant (Levy et al., 1985). At high elevation sites such as the Jet Propulsion Laboratory Table Mountain Facility in Southern California (TMF hereafter), the effect of the boundary layer is very small, and ozone variability is expected to be driven by transport processes from the stratosphere or horizontal transport within the troposphere (Cui et al., 2009; Naja et al., 2003; Trickl et al., 2010).

Several studies show that background ozone levels have increased significantly since preindustrial times (Mickley et al., 2001; Parrish et al., 2012; Staehelin et al., 1994; Volz and Kley, 1988) and these levels continued rising in the last decades in both Hemispheres (Derwent et al., 2007; Jaffe et al., 2004; Lee and Akimoto, 1998; Naja and Akimoto, 2004; Oltmans et al., 2006; Parrish et al., 2012; Simmonds et al., 2004; Tanimoto et al., 2009; Zbinden et al., 2006; Lelieveld et al., 2004). Nevertheless, after air quality regulations were implemented in the 1970s, the increasing trend has slowed down or is even reverted in regions such as the Eastern U.S. and Europe (Cooper et al., 2012, 2014; Granier et al., 2011). The situation is not the same for emerging economies such as Asia, where emissions are increasing with the corresponding increase in ozone levels (Dufour et al., 2010; Gao et al., 2005; Strode et al., 2015; Tie et al., 2009; Wang et al., 2006).

In most cases, variability and trend studies have revealed very large ozone variability with time, location and altitude (Cooper et al., 2014). This variability is mostly due to the large heterogeneity and variability of the ozone sources themselves, the different chemical processes affecting the formation and depletion of tropospheric ozone and its variable lifetime in the troposphere. Ozone atmospheric lifetime goes from a few hours in polluted boundary layer to

85   several weeks in the free troposphere, allowing it to travel over distances of intercontinental

86   scale (Stevenson et al., 2006; Young et al., 2013). In order to obtain statistically significant

87   results and be able to assess tropospheric ozone interannual variability and trends, a large long-

88   term monitoring dataset with global coverage is required, which has not yet been achieved

89   considering the current observation capabilities.

90   Long-term records of tropospheric ozone are available since the 1950s (Feister and Warmbt,

91   1987; Parrish et al., 2012), but it is not until the 1970s that the number of ozone monitoring

92   stations became significant (Cooper et al., 2014 and references therein). Currently, a

93   considerable number of ozone monitoring sites are operating as part of regional networks or

94   international programs (e.g. World Meteorological Observation Global Atmosphere Watch

95   WMO/GAW, Acid Deposition Monitoring Network in East Asia EANET, Clean Air Status and

96   Trends Network CASTNET, etc.). In addition to these ground-based networks, tropospheric

97   ozone measurements from satellite (TOMS, TES, OMI, etc.) or aircraft (MOZAIC/IAGOS)

98   platforms have been successfully implemented. Nevertheless, most of the tropospheric ozone

99   measurements are still only surface or column-integrated measurements whilst the number of

100 them with information on the vertical coordinate is very scarce. Until today, mainly ozonesonde

101 profiles have been used to provide altitude-resolved ozone variability information in the

102 troposphere (Logan, 1994; Logan et al., 1999; Naja and Akimoto, 2004; Oltmans et al., 1998,

103 2006, 2013), but the somewhat elevated cost of an ozonesonde launch has kept the sampling

104 interval to one profile per week (or less) for a given location. Differential Absorption Lidar

105 (DIAL) systems, which started to be used to measure tropospheric ozone in the late 1970s

106 (Bufton et al., 1979), complement the ozonesonde records, providing higher temporal resolution

107 thanks to their inherent operational configuration (from minutes to days of continuous

108 measurements). Today, tropospheric ozone lidars are still very scarce, but the implementation of

109 observation networks such as the international Network for the Detection of Atmospheric

110 Composition Change (NDACC, http://www.ndsc.ncep.noaa.gov), and more recently the North

111 American-based Tropospheric Ozone Lidar Network (TOLNet, http://www-

112 air.larc.nasa.gov/missions/TOLNet) allows for new capabilities that can contribute to the

113 understanding of processes affecting tropospheric ozone variability, and to satellite and model

114 validation and improvement.

Atmospheric
Chemistry
and Physics
Discussions

Open Access

EGU

115   As part of NDACC and TOLNet, a tropospheric ozone DIAL system located at TMF has

116   been operating since 1999. In this study, an analysis of 16 years of lidar profiles measured at the

117   station is presented together with the analysis of the surface ozone measurements available at the

118   site since 2013. The objective is to provide the first-ever published study of tropospheric ozone

119   variability above TMF using both the surface and lidar datasets. The work presented here is

120   particularly valuable due to the rising interest in the detection of long-term trends in the Western

121   United States (U.S.) and the scarcity of long-term measurements of ozone vertical profiles in this

122   region. The high terrain elevation and the deep planetary boundary layer of the intermountain

123   Western U.S. region facilitate inflow of polluted air masses originating in the Asian boundary

124   layer and ozone-rich stratospheric air down to the surface, thus highly influencing air quality in

125   the region (Brown-Steiner and Hess, 2011; Cooper et al., 2004; Langford et al., 2012; Liang et

126   al., 2004; Lin et al., 2012a, 2012b; Stohl, 2002). After a brief description of the instrumentation

127   and datasets (Section 2), an analysis of the seasonal and interannual variability of tropospheric

128   ozone above TMF for the period 2000-2015 will be presented in section 3. The study includes a

129   characterization of the air parcels sampled by lidar by identification of the source regions based

130   on backward trajectories analysis. A summary and discussion are provided in Section 4.

131   2.   Instrumentation

132   2.1 Tropospheric ozone lidar

133   TMF is located in the San Gabriel Mountains, in Southern California (34.4∘ N, 117.7∘ W), at an

134   elevation of 2285 m above sea level. Two differential absorption lidars (DIAL) and one Raman

135   lidar have been operating at the facility during nighttime typically four times per week, two

136   hours per night, contributing stratospheric ozone, temperature, tropospheric ozone, and water

137   vapor measurements to NDACC for several decades now. The original design in the mid-1990s

138   of the tropospheric ozone DIAL was optimized for tropospheric ozone and aerosol measurements

139   (McDermid, 1991). The system was later re-designed to provide exclusively tropospheric ozone

140   profiles (McDermid et al., 2002). The emitter uses a quadrupled Nd:YAG laser emitting two

141   beams at 266 nm. One beam is sent into a Raman cell filled with Deuterium to shift the

142   wavelength to 289 nm, the other beam is sent into another cell filled with Hydrogen to shift the

143   wavelength to 299 nm. The two beams are then expanded five times and transmitted into the

144   atmosphere. The light elastically backscattered in the troposphere (3-20 km) is collected by

Atmospheric
Chemistry
and Physics
Discussions

Open Access

145   several telescopes comprising mirrors of diameters varying from 91 cm diameter to 5 cm

146   diameter, thus accommodating for the large signal dynamic range implied when collecting light

147   from this close range. A total of three pairs of 289/299 nm channels is thus used to retrieve ozone

148   using the DIAL technique, each pair corresponding to a different intensity range and the

149   retrieved ozone profiles from all pairs combined together ultimately covering the entire

150   troposphere (3-18 km). As part of the retrieval process, the upper range of the ozone profile is

151   further extended to about 25 km by applying the DIAL technique on the 299 nm high intensity

152   channel of the tropospheric ozone lidar and the 355 nm low-intensity channel of the co-located

153   water vapor Raman lidar (Leblanc et al., 2012).

154   The instrument temporal sampling can be set to any value from a few seconds to several hours,

155   depending on the science or validation need. The vertical sampling can be set to any multiple of

156   7.5 m, again depending on the science or validation need. For the routine measurements

157   contributing to NDACC over the period 1999-2015 and used for the present work, the standard

158   settings have typically ranged between 5-min and 20-min for temporal sampling, and between

159   7.5 m and 75 m for the vertical sampling. Profiles routinely archived at NDACC are averaged

160   over 2-hours, with an effective vertical resolution varying from 150-m to 3 km, depending on

161   altitude. These temporal and vertical resolution settings yield a standard uncertainty of 7-14%

162   throughout the profile. The system operates routinely at nighttime, but daytime measurements

163   with reduced signal-to-noise ratio are occasionally performed in special circumstances such as

164   process studies, and aircraft or satellite validation. The total number of routine 2-hour ozone

165   profiles used in this study and archived at NDACC for the period 2000-2015 is included in Table

166   1.

167   The TMF ozone lidar measurements have been regularly validated using simultaneous

168   and co-located Electrochemical Concentration Cell (ECC) sonde measurements (Komhyr, 1969;

169   Smit et al., 2007). In the troposphere the precision of the ozonesonde measurement is around 3-

170   5%. TMF has ozonesonde launch capability since 2005 and 32 coincident profiles were obtained

171   over the period 2005-2013. Results from the lidar and the ECC comparison are included in

172   Figure 1. Figure 1c reveals that the deviations do not present significant changes with time,

173   which is an indicator of the system stability despite the multiple upgrades made over this time

174   period. In most cases, differences were within ±15% for the complete analyzed period. Note that

Atmospheric
Chemistry
and Physics
Discussions

175   a non-negligible fraction of the differences is due to geophysical variability. The measurement

176   geometry of the lidar and ozonesonde are radically different: 2-hour averaged, single location for

177   lidar, and horizontally-drifting instantaneous measurements for the ozonesonde.

178   2.2. Surface ozone measurements

179   Continuous surface ozone measurements have been performed at TMF since 2013 with a

180   UV photometric ozone analyzer (Model 49i from Thermo Fisher Scientific, US). The operation

181   principle is based on the absorption of UV light at 254 nm by the ozone molecules. The

182   instrument collects in-situ air samples at 2 meter above ground taken from an undisturbed

183   forested environment adjacent to the lidar building. It provides ozone mixing ratio values at 1-

184   minute time intervals with a lower detection limit of 1 ppbv.

185   3. Results

186

187   3.1.Surface ozone variability

188   Figure 2a shows the surface ozone seasonal cycle at TMF and nearby stations from the

189   California Air Resources Board (ARB) air quality network for the period 2013-2015. The

190   seasonal cycle at TMF comprises a maximum in spring and summer and a minimum in winter,

191   consistent with the ARB stations shown, as well as other stations in the US West Coast (e.g.

192   Schnell et al., 2015). Nonetheless, the seasonal cycle obtained at TMF from the hourly samples

193   (left plot) presents larger ozone values and lower variability throughout the year compared to the

194   other ARB stations. The mean surface value for the complete period at TMF is 55 ppbv, whereas

195   the seasonal values are 57, 57, 52 and 45 ppbv in spring (March-April-May), summer (June-July-

196   August), fall (September-October-November) and winter (December-January-February)

197   respectively. These values are in good agreement with those obtained from surface

198   measurements at high elevation sites in the Northern Hemisphere and reported in the review by

199   Cooper et al., (2014). When using the 8hMDA (8-h maximum daily average, right plot), larger

200   seasonal cycle amplitudes are observed, especially at stations affected by anthropogenic

201   pollution such as Crestline or San Bernardino. These polluted stations present larger values in

202   summer than those recorded at high-elevation remote stations like Joshua Tree or TMF. The

203   mean 8hMDA at TMF is 58 ppbv and the seasonal averages are 62, 66, 57 and 49 for spring,

204 summer, fall and winter respectively. The observed low seasonal variability is typical of high

205 elevation remote sites with low urban influence (Brodin et al., 2010). A similar behavior can be

206 observed at the Phelan, Joshua Tree or the Mojave National Preserve stations, all sites being at

207 high elevation with low or negligible urban influence. In Figure 2a a secondary minimum is

208 observed at TMF and most of the ARB nearby stations in July-August, followed by a secondary

209 maximum in fall.

210 In Figure 2a a clear combined effect of the altitude and proximity to anthropogenic pollution

211 sources on the ozone levels is observed. In general, higher ozone levels and lower variability are

212 observed at higher altitudes. The lowest altitude Pico Rivera instrument measures the lowest

213 ozone levels, and the highest-altitude TMF instrument measures the highest ozone levels

214 throughout the year when considering the hourly sampled dataset. A mean difference of ~30

215 ppbv is observed for a 2-km altitude difference. The magnitude of this positive ozone vertical

216 gradient depends on the distance from anthropogenic pollution sources. The effect of pollution is

217 clearer on the 8hMDA data, where high-elevation stations, yet more likely to be affected by

218 pollution such as Crestline or Victorville, present a larger seasonal cycle amplitude associated

219 with lower ozone levels in winter and higher levels in summer. A similar impact of the interplay

220 between urban influence and high-elevation was previously reported by Brodin et al., (2010).

221 The difference between the seasonal cycle retrieved from the 1-hour averaged data and the

222 8hMDA can be easily explained from the differences in the daily cycles at the different stations.

223 The mean surface ozone diurnal cycle at TMF and nearby ARB stations is shown in Figure 2b

224 for the four seasons. Minimum values are observed at nighttime, whereas maxima appear in late

225 afternoon. As for the seasonal cycle, the daily cycle at TMF, Joshua Tree, Mojave National

226 Preserve and Phelan stations exhibit low variability compared to the other stations located at

227 lower altitude and more affected by urban pollution. On average, daily values are larger at high

228 elevation remote sites as TMF or Joshua Tree. However, the afternoon maximum is larger at

229 polluted stations such as Crestline, especially in the summer season. In addition, the maximum at

230 TMF and the ARB stations of Joshua Tree and Mojave National Preserve occurs later than at the

231 other stations. The difference in timing is likely due to the different chemical species involved in

232 the ozone formation and depletion processes due to the low influence of anthropogenic pollution

233 (Brodin et al., 2010; Gallardo et al., 2000; Naja et al., 2003). In winter, a minimum is observed at

Atmospheric
Chemistry
and Physics
Discussions

234   TMF in the afternoon instead of the maximum observed at the other stations. This difference in

235   diurnal pattern has been observed at other remote or high-elevation sites and has been attributed

236   to the shorter day length and the lack of ozone precursors compared to urban sites. The resulting

237   daytime photochemical ozone formation is insufficient to produce an ozone diurnal variation

238   maximizing in the afternoon (Brodin et al., 2010; Gallardo et al., 2000; Naja et al., 2003;

239   Oltmans and Komhyr, 1986; Pochanart et al., 1999; Tsutsumi and Matsueda, 2000).

240   3.2.Tropospheric ozone variability

241   The red curve in Figure 3a (left plot) shows the average tropospheric ozone profile obtained by

242   the TMF lidar for the period 2000-2015. The cyan horizontal bars show the corresponding

243   standard deviation at 1-km interval. The red dot at the bottom of the profile shows the 2013-2015

244   mean surface ozone obtained from the data acquired simultaneously to the lidar measurements.

245   The lidar system can provide information from around 1.3 km (200 meters since 2013) above the

246   surface up to 25 km, covering the whole troposphere and the lower stratosphere. The average

247   mixing ratio value in the mid-troposphere is 55 ppbv. Above 8 km, the ozone mixing ratio

248   increases, reaching values above 1 ppmv at 16 km.

249   The seasonally averaged profiles are shown in Figure 3b. They show larger values in

250   spring and summer in the troposphere, whereas in the stratosphere maximum values are observed

251   in winter and spring. Within the troposphere, below 9 km, the seasonally-averaged profiles show

252   average values of 62, 60, 51 and 50 ppbv in spring, summer, fall and winter respectively. These

253   values are in good agreement with the average ozone concentrations (50-70 ppbv) obtained in

254   previous studies (Thompson et al., 2007; Zhang et al., 2010) above the western U.S. In the

255   altitude range 9-16 km (UTLS) a much larger variability in ozone is observed, as indicated by

256   the large standard deviation (left plot) and the differences between the seasonally-averaged

257   profiles (right plot). This large variability results from the horizontal and vertical displacement of

258   the tropopause above the site, causing the lidar to sound either the ozone-rich lowermost

259   stratosphere or the ozone-poor sub-tropical upper troposphere for a given altitude.

260   The 2D color contours of Figure 4 show the composite (2000-2015) monthly mean ozone

261   climatology measured by lidar (main panel, 4-20 km). A similar 2D color contour representation

262   was used just below the main panel to represent the composite (2013-2015) monthly mean

Atmospheric
Chemistry
and Physics
Discussions

263   surface ozone. The climatological tropopause height at TMF is also included in the main panel
264   (blue dotted line), with mean values ranging between 12 and 15 km. As discussed previously in
265   this paper, the tropopause height variability is the main cause of the larger standard deviation
266   observed in Figure 3a in this region. Between the surface and 9 km, a very consistent seasonal
267   pattern is observed, with maximum values in April-May and minimum values in winter. The
268   spring-summer maximum in the free-troposphere has been consistently observed at other stations
269   in Europe and North America and is attributed to photochemical production (Law et al., 2000;
270   Petetin et al., 2015; Zbinden et al., 2006). Above 9 km, the seasonal maximum is observed
271   earlier, i.e., in March and April between 10 and 12 km and February and March at higher
272   altitudes, consistent with the transition towards a dynamically-driven lower stratospheric regime.
273   At these altitudes, the ozone minimum is also displaced earlier in the year (August-October),
274   which is consistent with the findings of Rao et al. (2003) above Europe.

275   The TMF surface and lidar data are found to be very consistent, both in terms of seasonal
276   cycle phase and amplitude, and in term of absolute mixing ratio values. The mean value obtained
277   from the lidar measurements in the troposphere is very similar to the mean value obtained from
278   the surface measurements (around 55 ppbv).

279   The consistency between the lidar and the surface data was found not only for the
280   seasonal cycle obtained from the monthly averaged values, but also for the complete time series.
281   The degree of correlation between the lidar measurements at the lowest point and the surface
282   measurements was investigated. As mentioned before, the lidar cannot measure all the way down
283   to the surface. The first valid measurement occurs at around 3.5-4 km depending on the time
284   period. Therefore, the layer from 4 to 6 km is considered as the lower lidar layer. A correlation
285   coefficient of R=0.34 was found between the lidar data in the layer from 4 to 6 km and the
286   surface data. The correlation increases (R=0.44) if we consider a 3-hour time lag between the 4-6
287   km layer and the surface. After removing outliers corresponding to ozone values higher (or
288   lower) than the average plus (minus) one standard deviation either at the surface or at 4-6 km, the
289   correlation increases up to 0.69 for the simultaneous data and up to 0.79 for the 3-hour time-
290   shift.

291

292   3.3. Interannual variability and trends

293

Atmospheric
Chemistry
and Physics
Discussions

294   The 2000-2015 time-series of the deseasonalized ozone mixing ratio is shown in Figure

295   5. Anomalies, expressed in percent, were calculated by subtracting the climatological ozone

296   monthly mean profiles computed for the period 2000-2015 to the measured lidar profiles. Large

297   ozone variability with time is clearly observed, highlighting the difficulty to identify trends and

298   patterns. No clear mode of interannual variability is observed for the analyzed period here.

299   However, positive anomalies seem to predominate throughout the troposphere during the period

300   2003-2007, especially below 7 km. On average, ozone mixing ratio values in the lower

301   troposphere were 5 ppbv larger in 2003-2007 than during the entire period 2000-2015.

302   Following a procedure similar to that described in Cooper et al. (2012), a trend analysis

303   was performed at different altitude levels (Tables 2 and 3 and Figure 6). Figure 6 shows the time

304   series of the median, 95th and 5th percentile values, obtained every year between 2000 and 2015

305   for different layers and different seasons using the lidar profiles measured at TMF. In order to

306   obtain the trends, linear fits (shown in Figure 6) of the median, 95th and 5th percentiles were

307   performed independently using the least squares method. The ozone rate of change in ppbv.year^{-1}

308   was determined from the slope of the linear fit. To assess the significance of the trends, the F-

309   statistic test was used, with the p-Value as an indicator of the statistical significance. For p-

310   Values lower than 0.1, trends were assumed statistically significant, with a confidence level

311   larger than 90%.

312   The calculated trends were found to depend on altitude and season. Table 2 contains the

313   ozone rate change expressed in ppbv.year^{-1} (and %.year^{-1}) for the different layers and seasons for

314   the median, 5th and 95th percentiles. The corresponding standard errors and p-Values are included

315   in Table 3. Statistically significant trends are marked in bold font. The layer corresponding to the

316   upper troposphere (7-10 km) shows a statistically significant ozone increase of 0.31 ppbv.year^{-1}

317   (0.57%·year^{-1}) for the median values and 0.55 ppbv.year^{-1} (0.54%.year^{-1}) for the 95th percentile,

318   indicating that both the background and the high intensity events ozone levels were increasing

319   (Cooper et al., 2012, 2014). A similar increase in the free troposphere and in the western US was

320   reported by Cooper et al. (2012) for the period 1990-2010 for both the median and 95th

321   percentiles.

322   Now looking at each season separately, a significant positive trend was found in the

323   upper troposphere (7-10 km) for both spring and summer, with an ozone increasing rate of 0.71

324   and 0.58 ppbv.year^{-1} respectively (or 1.10 and 0.98%·year^{-1}), and an ozone decrease of -0.43

Atmospheric
Chemistry
and Physics
Discussions

325   ppbv.year^{-1} (-0.87%·year^{-1}) during winter. Statistically significant trends were also found in the

326   lower troposphere (4-7 km) during winter for the median and 5th percentile values with an ozone

327   decrease of -0.36 ppbv.year^{-1} and -0.59 ppbv.year^{-1} respectively (-0.72 and -1.53%·year^{-1}

328   respectively) (Table 2). No significant trend was observed near the tropopause (12-16 km),

329   whereas a significant negative trend of -8.79 ppbv.year^{-1} (-1.39%·year^{-1}) for the median and -

330   5.80 ppbv.year^{-1} (-1.26%·year^{-1}) for the 5th percentile in fall was observed in the lower

331   stratosphere (17-19 km).

332   3.4. Characterization of the air masses sounded by the TMF tropospheric ozone lidar

333   In an attempt to characterize the air parcels sounded by lidar above TMF based on their travel

334   history, 8-day backward trajectories ending at TMF between 5 and 14 km altitude were

335   computed using the HYSPLIT4 model (Draxler and Rolph, 2003),

336   http://www.arl.noaa.gov/ready/hysplit4.html). The NCAR/NCEP Reanalysis Pressure level data

337   were used as meteorological input (Kalnay and Kanamitsu, 1996) in HYSPLIT4. These data,

338   available since 1948, provide 4-times-daily meteorological information at 17 pressure levels

339   between the 1000 and 10 hPa and 2.5x2.5 degrees horizontal resolution. Several studies (Harris

340   et al., 2005; Stohl, 1998) provided a wide range of uncertainty estimates along the trajectories.

341   The more recent study by Engström and Magnusson, (2009) indicate values of 354-400 km

342   before 4 days and 600 km after.

343   Our trajectory analysis comprises two steps. First, the 8-day backward trajectories computed

344   by HYSPLIT and ending at different altitude levels were grouped using the HYSPLIT clustering

345   tool (Draxler et al., 2009) in order to identify the most significant paths followed by the air

346   masses arriving over the station. Based on the results of this preliminary analysis, five main

347   regions were identified: the stratosphere, the Asian boundary layer (ABL), the free-troposphere

348   above Asia (AFT), Central America, and the Pacific Ocean. Once these geographical areas were

349   identified, we performed a classification of the air parcels according to the criteria described

350   next.

351   An air parcel was classified as "stratospheric" if the 8-day backward trajectory intercepted

352   the tropopause and resided at least 2 days above the local tropopause. The tropopause height

353   information comes from the global tropopause height data derived once a day by the NOAA

Atmospheric
Chemistry
and Physics
Discussions

Open Access

EGU

354   Physical Sciences Division (http://www.esrl.noaa.gov/psd) from the same NCAR/NCEP

355   Reanalysis database used as input to HYSPLIT4. Computations are based on the World

356   Meteorological Organization (WMO, 1957) definition, that is, the lowest height at which the

357   temperature lapse rate becomes lower than 2 $K \cdot km^{-1}$, provided that along 2 km above this height

358   the average lapse is also lower than 2 $K \cdot km^{-1}$. In addition, the NOAA computations do not allow

359   tropopause heights at pressure levels larger than 450 hPa and smaller than 85 hPa.

360   Next, the air parcels that were not classified as "stratosphere" were then classified as "Asian

361   boundary layer" (ABL) for trajectories comprising a minimum residence time of 2 days within

362   the area labelled "ABL" in Figure 7, and below an altitude of 3 km. Next, air parcels with

363   trajectories comprising a minimum residence time of 2 days within the area labelled "AFT" in

364   Figure 7, and above 3 km altitude were classified as "Asian Free-troposphere" (AFT).

365   The air parcels not classified as "stratosphere", "ABL", or "AFT" were then classified as

366   "Central America" if the corresponding trajectories' residence time over the "Central America"

367   region depicted in Figure 7 was found to be at least 2 days. Finally, the remaining parcels were

368   classified as "Pacific Ocean" when the residence time above the corresponding region (see figure

369   7) reached or exceeded 2 days.

370   The classification of the air parcels took place sequentially, which means that each

371   category is exclusive of the others. The classification was made for each of the four seasons

372   separately in order to account for the seasonal changes in synoptic circulation. Examples of the

373   corresponding classified back-trajectories are shown in Figure 8. The number and frequency of

374   occurrences of each air parcel category for all seasons is compiled in Table 4. A monthly

375   distribution of these occurrences is shown in Figure 9. With the selection criteria we have set, a

376   very low number of parcels classified "ABL" were found. Air parcels dominantly originate in the

377   Pacific Ocean below 10 km, with almost equal influence throughout the year. Increasing

378   influence of the stratosphere is observed at upper levels, with values ranging between 2 to 78%

379   or higher during winter and spring. This result agrees well with previous studies in the Western

380   US (Sprenger, 2003; Stohl, 2003). A statistically significant Central American influence was

381   identified in summer with a frequency of occurrence varying between 11% and 3%, decreasing

382   with altitude. The Central America influence coincides with the establishment of the North

Atmospheric
Chemistry
and Physics
Discussions

383   American Monsoon circulation from July to September and which affects Central America and

384   the Southwestern US.

385   Composite ozone profiles and statistical parameters were estimated for each category of

386   air parcel and for altitudes between 4.5 and 13.5 km at 1-km altitude intervals. Figure 10 shows

387   the ozone mixing ratio mean (open circles), median (red bars), 25th and 75th percentiles (blue

388   bars) at 9 km altitude for each of the identified categories and season. The number of

389   occurrences for each category is mentioned between parentheses. The ozone statistics obtained

390   when a low number of occurrences was found should be ignored (e.g., Central America in

391   Spring, or ABL for most seasons). Figure 11 shows, for each season, the composite ozone

392   profiles constructed from the ozone mixing ratio median values found for a particular category at

393   a given altitude. In order to keep the most statistically significant results, composite values

394   computed using less than 5% of the total number of samples for a given season were not plotted,

395   leaving out certain sections of the composite profiles, and in the case of ABL, leaving out the

396   entire profile.

397   Not surprisingly, the analysis reveals that larger ozone mixing ratio values were observed

398   when the air masses were classified as "stratospheric" regardless of altitude and season (65-85

399   ppbv below 9 km). For this category, large ozone variability was found, as indicated by the 25th

400   and 75th percentiles in Figure 10. As altitude increases, the influence of the stratosphere is more

401   important, exceeding 30% above 12 km, resulting in higher ozone mixing ratio values (red

402   curves in Figure 11).

403   Conversely, low ozone mixing ratio values (50-65 ppbv below 9 km) were consistently

404   associated with the air parcels classified as "Pacific Ocean" (cyan curves). This region can be

405   considered as a source of 'background ozone', since no anthropogenic source is expected to

406   affect the local ozone budget. Slightly higher ozone content (50-70 ppbv higher) is

407   systematically found for air parcels classified as "AFT", but the number of occurrences remains

408   too small to provide any meaningful interpretation. No conclusion can be made for air parcels

409   classified as "ABL" due to the very low number of occurrences found.

410   During summer, ozone values of about 70 ppbv were found at 9 km altitude for the 85 air

411   parcels classified as "Central America" (yellow curve). The corresponding values for the 277 air

Atmospheric
Chemistry
and Physics
Discussions

412 parcels classified as "Pacific Ocean" are about 55 ppbv, which is 15 ppbv lower. This difference

413 possibly points out to the lightning-induced enhancement of ozone within the more frequent

414 occurrence of thunderstorms during the North American summer monsoon.

415   3.5. The influence of tropopause folds on the TMF tropospheric ozone record

416 In the previous section, a large variability in the composite ozone content was found for the air

417 parcels classified as "stratospheric". In the current section, we provide at least one clear

418 explanation for this large variability. Tropopause folds are found primarily in the vicinity of the

419 subtropical jets, in the 20º-50º latitude range. They typically consist of three-dimensional folds of

420 the virtual surface separating air masses of tropospheric characteristics (weakly stratified, moist,

421 low ozone concentration, etc.) and those of stratospheric characteristics (highly stratified, dry,

422 high ozone concentration, etc.). Tropopause folds can result in the transport of large amounts of

423 stratospheric ozone into the troposphere, reaching in some cases the planetary boundary layer

424 and enhancing ozone amounts even at the surface (Chung and Dann, 1985; Langford et al., 2012;

425 Lefohn et al., 2012; Lin et al., 2012a). They are considered one of the main mechanisms of

426 stratosphere-to-troposphere exchange and have been widely studied in the past (e.g. Bonasoni

427 and Evangelisti, 2000; Danielsen and Mohnen, 1977; Lefohn et al., 2011; Vaughan et al., 1994;

428 Yates et al., 2013). Due to the location of TMF, the upper troposphere above the site is

429 frequently impacted by tropopause folds. The MERRA reanalysis (1-km vertical resolution, 1 x

430 1.25 degrees horizontal resolution) were used in this study to identify the presence of double

431 tropopauses above the station. A comparison between the MERRA temperature profiles and the

432 temperature profiles measured by the radiosondes launched at TMF was performed in order to

433 evaluate the performance of MERRA above TMF. The comparison (not shown) reveals excellent

434 agreement, with average relative differences of 2% or less from the surface up to 25 km. The

435 heights of double tropopauses were computed following a methodology similar to that proposed

436 in Chen et al., (2011). The first (lower) tropopause is identified according to the WMO

437 definition, as explained earlier. A second (upper) tropopause is identified above the WMO

438 tropopause if the temperature lapse rate increases over 3 K·km^{-1} within at least 1 km, and its

439 height is determined once again by the WMO criterion.

440   Using this methodology, we found that 27% of the TMF tropospheric ozone lidar profiles

441 were measured in the presence of double tropopauses. Figure 12 shows the number of cases with

Atmospheric
Chemistry
and Physics
Discussions

442 double tropopauses above TMF distributed per months, with the number of days with tropopause

443 folds being normalized to the total number of measurements every month (compiled in Table 1).

444 As we can see, the presence of double tropopauses was especially frequent during winter and

445 spring, which coincides with the higher frequency of stratospheric air masses arriving at TMF

446 estimated by the backward trajectories analysis (Figure 9). The altitude of detected single

447 tropopauses is found around 13 km in winter and spring, and 16-17 km in summer and fall

448 (Figure 13a-d). When a double tropopause is identified, the altitude of the lower tropopause

449 ranges between 8 and 15 km, with the distribution peak centered around 12-13 km (Figure 13e-

450 h), and the second tropopause is detected typically around 17-18 km (Figure 13i-l).

451 Figure 14 shows the average of all tropospheric ozone lidar profiles measured in winter

452 (blue curves) and spring (red curves) in the presence of a double tropopause (solid curves), and

453 in the presence of a single tropopause (dashed curves). The right panel (Figure 14b) is simply a

454 lower tropospheric-zoomed version of the left panel (Figure 14a). Only winter and spring are

455 shown because they are the seasons most affected by double tropopause cases as previously

456 stated. In the presence of double tropopauses a clear dual vertical structure in ozone is observed,

457 with higher ozone values between 12 and 14 km and lower mixing ratio values between 14 and

458 18 km. In the case of deep stratospheric intrusions, ozone-rich stratospheric air masses embedded

459 in the lower half of the fold can reach lower altitudes, and occasionally the planetary boundary

460 layer mixing down to the surface (Chung and Dann, 1985; Langford et al., 2012, 2015; Lefohn et

461 al., 2012; Lin et al., 2012a), leading to an ozone increase in the lower troposphere (Figure 14b).

462 In our case, the mean increase is around 2 ppbv below 6 km for both spring and winter. Note the

463 relative magnitude of the ozone anomalies in the lower and upper halves of the fold is different

464 for spring and winter. A detailed investigation, beyond the scope of the present work, is needed

465 to assess the actual significance of this difference.

466 4. Discussion

467 The present study allowed the characterization of the full tropospheric ozone profile from the

468 ground to the stratosphere, and is particularly valuable in the context of a notoriously sparse

469 horizontal coverage for this type of vertically resolved measurements in a region affected by

470 transboundary ozone inflow and stratospheric intrusions.

Atmospheric
Chemistry
and Physics
Discussions

471   The combined analysis of the surface measurements and the simultaneous lidar profiles

472   reveals high consistency between the ozone at the surface and in the free troposphere. This

473   consistency may point out the fact that the TMF surface measurements are representative of the

474   lower part of the free troposphere (i.e., below 7 km), at least during the nighttime lidar

475   measurements. Additional daytime lidar measurements will be performed in 2016 to assess

476   whether such consistency also exists at other times of the day, especially in the afternoon.

477   The analysis of the long-term lidar time-series (16 years covered) shows no significant

478   signatures of interannual variability, as previously discussed. More importantly, no obvious

479   signature of ENSO or the QBO could be identified, which is inconsistent with the recent findings

480   of Lin et al., (2015) or Neu et al., (2014), who have linked tropospheric ozone variability in the

481   Northern Hemisphere to El Niño/ La Niña events, and the QBO, through the variations of

482   stratospheric/tropospheric ozone fluxes. However, this inconsistency might not be so surprising

483   if we take into account the obvious difference in measurement sampling (one single location in

484   the Western U.S. as opposed to global observations).

485   Nevertheless, our analysis reveals statistically-significant trends for selected seasons and

486   altitudes. Specifically, a positive trend of 0.31 ppbv.year^{-1} (ozone annual median) was found in

487   the upper troposphere (7-10 km). This positive trend is more pronounced in spring and summer

488   (0.71 and 0.58 ppbv.year^{-1} respectively), while a negative trend (-0.43 ppbv.year^{-1}) was found in

489   winter. The positive trend obtained here in spring for the median values is larger than the trend

490   obtained by Cooper et al. (2012) for the free troposphere in 1995-2011 (0.41 ppbv.year^{-1}), and

491   even larger than the trend obtained by Lin et al. (2015b) using model data (0.37 ppbv.year^{-1}

492   during 1995-2012). This disagreement could be due to differences in sampling, as concluded in

493   Lin et al. (2015b). Nonetheless, Figure 6 shows larger ozone median (and 5th and 95th percentile)

494   values at 7-10 km in 2013-2015 than in preceding years, with this period not being included in

495   the previous studies. A lower ozone increasing rate in 2000-2012 above TMF (0.43 ppbv.year^{-1})

496   suggests that that the ozone rate of change has increased in the last years, but a more

497   comprehensive study with regional coverage would be necessary to confirm this change.

498   Regarding winter season, a positive trend was obtained on a regional scale in Cooper et al.,

499   (2012), but certain sites in the western U.S. showed a negative trend, as in our case. This

500   negative trend indicates a decrease in the background ozone values. During winter months, a

Atmospheric
Chemistry
and Physics
Discussions

501   smaller influence of transboundary ozone transport is expected at low altitudes above TMF and

502   the decrease in background ozone during these months could be associated with the decrease in

503   domestic anthropogenic emissions.

504   The springtime positive trend estimates reported in the Western US oppose ozone

505   decrease in the Eastern part. These results indicate that the two-decade-long efforts to implement

506   regulations to control air quality and anthropogenic emissions in the U.S. have led to a clear

507   decrease in ozone levels in the Eastern U.S., but not in the Western U.S. (e.g. Copper et al.,

508   2012; 2014). This different regional behavior has been attributed to the inflow of elevated ozone,

509   mainly from East Asia, and to the increasing contribution of stratospheric intrusions (Cooper et

510   al., 2010; Jacob et al., 1999; Parrish et al., 2009; Reidmiller et al., 2009). But again, differences

511   in sampling can impact significantly the interpretation of our trend estimates. As pointed out by

512   Lin et al. (2015b), further coordination efforts at both global and regional scales are necessary in

513   order to reduce biases introduced by inhomogeneity in sampling. As part of these efforts, an

514   extended analysis based on the origin of the air masses sampled by the TMF lidar is under way,

515   with the ultimate objective to filter synoptic noise out, and better quantify the ENSO and QBO

516   signals and the residual trends. As a prerequisite to such study, a preliminary characterization of

517   the air masses sounded by the TMF lidar was performed and presented here.

518   Backward trajectories analysis reveals that, not surprisingly, parcels identified as

519   "stratosphere" contain the highest ozone mixing ratios, and parcels classified as "Pacific Ocean"

520   contain the lowest ozone concentrations, which can be considered as 'background conditions'.

521   Despite influence of Asian pollution in the ozone levels in the Western US has been detected in

522   previous studies (e.g. Zhang et al., 2008; Lin et al., 2012; Langford et al., 2015), no outstanding

523   signature from the Asian boundary layer could be identified due to the low number occurrences

524   associated with this category in our case. Nevertheless, air parcels classified as "Asian free-

525   troposphere" seemed to contain systematically more ozone than those classified as "Pacific

526   Ocean", especially below 9 km. A refined classification, probably requiring the use of chemistry-

527   transport models, is needed to assess whether the Asian boundary layer or the Asian free-

528   troposphere have a detectable impact on the ozone content measured above TMF.

529   In summer, air masses coming from Central America were frequently detected. The

530   ozone mixing ratio values measured in this case were clearly above the climatological mean,

Atmospheric
Chemistry
and Physics
Discussions

Open Access

EGU

531   with values up to 15 ppbv larger than those associated with the Pacific Ocean region. Previous

532   studies (Cooper et al., 2009), have observed enhanced ozone values associated with the North

533   American Monsoon, mainly due to ozone production associated with lightning (Choi et al., 2009;

534   Cooper et al., 2009). However, this feature was observed in the Eastern U.S. Because of the

535   synoptic conditions during the monsoon, the Western U.S. is not as much influenced and no

536   significant ozone increase was reported (Barth et al., 2012; Cooper et al., 2009). Nevertheless,

537   Cooper et al., (2009) reported higher modeled lightning-induced NO_x concentrations at TMF

538   than at other western locations, which would be consistent with our findings. Further

539   investigation, including a detailed history of the meteorological conditions along the trajectories,

540   is needed to confirm this correlation.

541   As part of the characterization of the TMF lidar-sampled air masses, the impact of double

542   tropopauses was assessed. Between 2000 and 2015, the frequency of occurrence of double

543   tropopauses above TMF was found to be around 27%. This high frequency, especially observed

544   in winter and spring, was expected considering the latitude of TMF, i.e., near the subtropical jet,

545   where frequent tropopause folds occur. More interestingly, a clear, dual vertical structure in

546   ozone was observed in the presence of a double tropopause (Figure 14). The double tropopause

547   is expected to result from a tropopause fold in the layer between the two identified tropopauses.

548   The dual ozone structure observed by lidar coincides with the expected location of the fold, and

549   consists of systematically higher-than-average mixing ratios in the lower half of the fold (12-14

550   km), and lower-than-average mixing ratios in the upper half of the fold (14-18 km). This dual

551   structure is consistent with the expected origin of the air masses within a tropopause fold.

552   Stratospheric air, richer in ozone, is measured within the lower half of the fold, while

553   tropospheric ozone-poor air is measured within the upper half of the fold. In addition,

554   statistically significant higher-than-average mixing ratios (+2 ppbv) are observed in the lower

555   troposphere (4-10 km) in the presence of double-tropopauses. This increase is consistent with

556   previous reports of the importance of the stratosphere as an ozone source in the lower

557   troposphere (Cooper and Stohl, 2005; Langford et al., 2012; Lefohn et al., 2011; Trickl et al.,

558   2011), with a 25 to 50% contribution to the tropospheric budget (Davies and Schuepbach, 1994;

559   Ladstätter-Weißenmayer et al., 2004; Roelofs and Lelieveld, 1997; Stevenson et al., 2006).

Atmospheric
Chemistry
and Physics
Discussions

560   Further investigation is now underway, with the objective of better identifying all

561   signatures of interannual variability and trends. This long-term variability investigation not only

562   will include an air mass classification based on geographical area, but will also take into account

563   the history of the air parcels in the context of nearby tropopause folds. Altogether, this air parcel

564   characterization, used in conjunction with regional chemistry-climate or chemistry-transport

565   model runs, should unveil signatures hidden in the current lidar record, and eventually shed new

566   light on the origin of the reported past, current, and future tropospheric ozone trends over the

567   Western U.S.

568   5. Concluding remarks

569   Combined ozone photometer surface measurements (2013-2015) and tropospheric ozone

570   DIAL profiles (2000-2015) at the JPL-Table Mountain Facility were presented for the first time.

571   The high ozone values and low interannual and diurnal variability measured at the surface,

572   typical of high elevation remote sites with no influence of urban pollution, constitute a good

573   indicator of background ozone conditions over the Southwestern US.

574   The 16-year tropospheric ozone lidar time-series is one of the longest lidar records

575   available and is a valuable dataset for trend analysis in the Western US, where the number of

576   long-term observations with high vertical resolution in the troposphere is very scarce. A

577   statistically significant positive trend was observed in the upper troposphere, in agreement with

578   previous studies. This ozone increase points out to the influence of long-range transport and/or a

579   change in stratospheric influence, since ozone precursor emissions have been decreasing in the

580   US over the past two decades.

581   Ozone vertical distribution above TMF is affected by the frequent occurrence of

582   tropopause folds. A dual vertical structure in ozone within the fold layer was clearly observed,

583   characterized by above-average values in the bottom half of the fold (12-14 km), and below-

584   averaged values in the top half of the fold (14-18 km). Above-average ozone values were also

585   observed near the surface (+2 ppbv) on days with a tropopause fold. The high frequency of

586   tropopause folds observed above the site is not surprising given Table Mountain's position in the

587   vicinity of the subtropical jet. A detailed and systematic analysis of the ozone vertical structure,

588   and its variability in relation to the proximity of the subtropical jet is in preparation. This

Atmospheric
Chemistry
and Physics
Discussions

589 analysis, which will utilize a large amount of model data together with the lidar observations,

590 should shed some light on a possible correlation between the observed upper tropospheric ozone

591 positive trends and the impact of the tropopause folds, either as a result of an increase in

592 frequency of the stratospheric intrusions, or as a result of the mid-latitude stratospheric ozone

593 recovery observed since the early 2000s (WMO, 2014).

594

595 ACKNOWLEDGEMENTS

608 REFERENCES

609 Ambrose, J., Reidmiller, D. and Jaffe, D.: Causes of high O 3 in the lower free troposphere over the
610 Pacific Northwest as observed at the Mt. Bachelor Observatory, Atmos. Environ., 2011.

611 Barth, M. C., Lee, J., Hodzic, A., Pfister, G., Skamarock, W. C., Worden, J., Wong, J. and Noone, D.:
612 Thunderstorms and upper troposphere chemistry during the early stages of the 2006 North American
613 Monsoon, Atmos. Chem. Phys., 12(22), 11003–11026, doi:10.5194/acp-12-11003-2012, 2012.

614 Bonasoni, P. and Evangelisti, F.: Stratospheric ozone intrusion episodes recorded at Mt. Cimone during
615 the VOTALP project: case studies, Atmos. Environ, *34*(9), 1355-1365, 2000.

616 Brodin, M., Helmig, D. and Oltmans, S.: Seasonal ozone behavior along an elevation gradient in the
617 Colorado   Front   Range   Mountains,   Atmos.   Environ.,   44(39),   5305–5315,
618 doi:10.1016/j.atmosenv.2010.06.033, 2010.

Atmospheric
Chemistry
and Physics
Discussions

619 Brown-Steiner, B. and Hess, P.: Asian influence on surface ozone in the United States: A comparison of
620 chemistry, seasonality, and transport mechanisms, J. Geophys. Res., 116(17), 1–13,
621 doi:10.1029/2011JD015846, 2011.

622 Bufton, J. L., Stewart, R. W. and Weng, C.: Remote measurement of tropospheric ozone., Appl. Opt.,
623 18(20), 3363–4, doi:10.1364/AO.18.003363, 1979.

624 Choi, Y., Kim, J., Eldering, A., Osterman, G., Yung, Y. L., Gu, Y. and Liou, K. N.: Lightning and
625 anthropogenic NOx sources over the United States and the western North Atlantic Ocean: Impact on
626 OLR and radiative effects, Geophys. Res. Lett., 36(17), L17806, doi:10.1029/2009GL039381, 2009.

627 Chung, Y. and Dann, T.: Observations of stratospheric ozone at the ground level in Regina, Canada,
628 Atmos. Environ., *19*(1), 157-162, 1985.

629 Cooper, O. and Stohl, A.: A springtime comparison of tropospheric ozone and transport pathways on the
630 east and west coasts of the United States, J. Geophys. Res., 110(D5), 2005.

631 Cooper, O. R., Forster, C., Parrish, D., Trainer, M., Dunlea, E., Ryerson, T., Hübler, G., Fehsenfeld, F.,
632 Nicks, D., Holloway, J., de Gouw, J., Warneke, C., Roberts, J. M., Flocke, F. and Moody, J.: A case study of
633 transpacific warm conveyor belt transport: Influence of merging airstreams on trace gas import to North
634 America, J. Geophys. Res., 109(D23), n/a–n/a, doi:10.1029/2003JD003624, 2004.

635 Cooper, O. R., Eckhardt, S., Crawford, J. H., Brown, C. C., Cohen, R. C., Bertram, T. H., Wooldridge, P.,
636 Perring, A., Brune, W. H., Ren, X., Brunner, D. and Baughcum, S. L.: Summertime buildup and decay of
637 lightning NO $_x$ and aged thunderstorm outflow above North America, J. Geophys. Res., 114(D1), D01101,
638 doi:10.1029/2008JD010293, 2009.

639 Cooper, O. R., Parrish, D. D., Stohl, A., Trainer, M., Nédélec, P., Thouret, V., Cammas, J. P., Oltmans, S. J.,
640 Johnson, B. J., Tarasick, D., Leblanc, T., McDermid, I. S., Jaffe, D., Gao, R., Stith, J., Ryerson, T., Aikin, K.,
641 Campos, T., Weinheimer, A. and Avery, M. A.: Increasing springtime ozone mixing ratios in the free
642 troposphere over western North America, Nature, 463(7279), 344–348, doi:10.1038/nature08708, 2010.

643 Cooper, O. R., Gao, R.-S., Tarasick, D., Leblanc, T. and Sweeney, C.: Long-term ozone trends at rural
644 ozone monitoring sites across the United States, 1990-2010, J. Geophys. Res., 117(D22), n/a–n/a,
645 doi:10.1029/2012JD018261, 2012.

646 Cooper, O. R., Parrish, D. D., Ziemke, J., Balashov, N. V., Cupeiro, M., Galbally, I. E., Gilge, S., Horowitz, L.,
647 Jensen, N. R., Lamarque, J.-F., Naik, V., Oltmans, S. J., Schwab, J., Shindell, D. T., Thompson, A. M.,
648 Thouret, V., Wang, Y. and Zbinden, R. M.: Global distribution and trends of tropospheric ozone: An
649 observation-based review, Elem. Sci. Anthr., 2, 000029, doi:10.12952/journal.elementa.000029, 2014.

650 Cui, J., Sprenger, M., Staehelin, J., Siegrist, A., Kunz, M., Henne, S. and Steinbacher, M.: Impact of
651 stratospheric intrusions and intercontinental transport on ozone at Jungfraujoch in 2005: comparison
652 and validation of two Lagrangian approaches, Atmos. Chem. Phys., 9(10), 3371–3383, doi:10.5194/acp-
653 9-3371-2009, 2009.

654 Danielsen, E. F. and Mohnen, V. A.: Project dustorm report: ozone transport, in situ measurements, and
655 meteorological analyses of tropause folding, J. Geophys. Res., 82(37), 5867–5877,
656 doi:10.1029/JC082i037p05867, 1977.

657 Davies, T. D. and Schuepbach, E.: Episodes of high ozone concentrations at the earth's surface resulting
658 from transport down from the upper troposphere/lower stratosphere: a review and case studies,
659 Atmos. Environ., 28(1), 53–68, doi:10.1016/1352-2310(94)90022-1, 1994.

Atmospheric
Chemistry
and Physics
Discussions

Open Access

EGU

660 Derwent, R. G., Simmonds, P. G., Manning, A. J. and Spain, T. G.: Trends over a 20-year period from 1987
661 to 2007 in surface ozone at the atmospheric research station, Mace Head, Ireland, Atmos. Environ.,
662 41(39), 9091–9098, doi:10.1016/j.atmosenv.2007.08.008, 2007.

663 Draxler, R., Stunder, B., Rolph, G. and Taylor, A.: Hysplit 4 User's Guide, NOAA Air Resources Laboratory,
664 Silver Spring, 2009.

665 Dufour, G., Eremenko, M., Orphal, J. and Flaud, J.-M.: IASI observations of seasonal and day-to-day
666 variations of tropospheric ozone over three highly populated areas of China: Beijing, Shanghai, and Hong
667 Kong, Atmos. Chem. Phys., 10(8), 3787–3801, doi:10.5194/acp-10-3787-2010, 2010.

668 Feister, U. and Warmbt, W.: Long-term measurements of surface ozone in the German Democratic
669 Republic, J. Atmos. Chem., 5(1), 1–21, doi:10.1007/BF00192500, 1987.

670 Forster, P., Ramaswamy, V., Artaxo, P., Bernstsen, T., Betts, R., Fahey, D. W., Haywood, J., Lean, J., Lowe,
671 D. W., Myhre, G., Nganga, J., Prinn, R., Raga, G., Schulz, M. and Van Dorland, R.: Changes in atmospheric
672 constituents and in radiative forcing. Chapter 2, Cambridge University Press, Cambridge, United
673 Kingdom and New York, NY, USA., 2007.

674 Gallardo, L., Carrasco, J. and Olivares, G.: An analysis of ozone measurements at Cerro Tololo (30
675 degrees S, 70 degrees W, 2200 m.a.s.l.) in Chile, Tellus B, 52(1), 50–59, doi:10.1034/j.1600-
676 0889.2000.00959.x, 2000.

677 Gao, J., Wang, T., Ding, A. and Liu, C.: Observational study of ozone and carbon monoxide at the summit
678 of mount Tai (1534m a.s.l.) in central-eastern China, Atmos. Environ., 39(26), 4779–4791,
679 doi:10.1016/j.atmosenv.2005.04.030, 2005.

680 Granier, C., Bessagnet, B., Bond, T., D'Angiola, A., Denier van der Gon, H., Frost, G. J., Heil, A., Kaiser, J.
681 W., Kinne, S., Klimont, Z., Kloster, S., Lamarque, J.-F., Liousse, C., Masui, T., Meleux, F., Mieville, A.,
682 Ohara, T., Raut, J.-C., Riahi, K., Schultz, M. G., Smith, S. J., Thompson, A., van Aardenne, J., van der Werf,
683 G. R. and van Vuuren, D. P.: Evolution of anthropogenic and biomass burning emissions of air pollutants
684 at global and regional scales during the 1980–2010 period, Clim. Change, 109(1-2), 163–190,
685 doi:10.1007/s10584-011-0154-1, 2011.

686 Jacob, D. J., Logan, J. A. and Murti, P. P.: Effect of rising Asian emissions on surface ozone in the United
687 States, Geophys. Res. Lett., 26(14), 2175–2178, doi:10.1029/1999GL900450, 1999.

688 Jaffe, D., Bertschi, I., Jaeglé, L., Novelli, P., Reid, J. S., Tanimoto, H., Vingarzan, R. and Westphal, D. L.:
689 Long-range transport of Siberian biomass burning emissions and impact on surface ozone in western
690 North America, Geophys. Res. Lett., 31(16), L16106, doi:10.1029/2004GL020093, 2004.

691 Ladstätter-Weißenmayer, A., Meyer-Arnek, J., Schlemm, A. and Burrows, J. P.: Influence of stratospheric
692 airmasses on tropospheric vertical O_3 columns based on GOME (Global Ozone Monitoring Experiment)
693 measurements and backtrajectory calculation over the Pacific, Atmos. Chem. Phys., 4(4), 903–909,
694 doi:10.5194/acp-4-903-2004, 2004.

695 Langford, A. O., Brioude, J., Cooper, O. R., Senff, C. J., Alvarez, R. J., Hardesty, R. M., Johnson, B. J. and
696 Oltmans, S. J.: Stratospheric influence on surface ozone in the Los Angeles area during late spring and
697 early summer of 2010, J. Geophys. Res., 117(D21), n/a–n/a, doi:10.1029/2011JD016766, 2012.

698 Langford, A. O., Pierce, R. B. and Schultz, P. J.: Stratospheric intrusions, the Santa Ana winds, and
699 wildland fires in Southern California, Geophys. Res. Lett., n/a–n/a, doi:10.1002/2015GL064964, 2015.

700 Law, K. S., Plantevin, P.-H., Thouret, V., Marenco, A., Asman, W. A. H., Lawrence, M., Crutzen, P. J.,

Atmospheric
Chemistry
and Physics
Discussions

701 Muller, J.-F., Hauglustaine, D. A. and Kanakidou, M.: Comparison between global chemistry transport
702 model results and Measurement of Ozone and Water Vapor by Airbus In-Service Aircraft (MOZAIC) data,
703 J. Geophys. Res., 105(D1), 1503, doi:10.1029/1999JD900474, 2000.

704 Leblanc, T., McDermid, I. S. and Walsh, T. D.: Ground-based water vapor raman lidar measurements up
705 to the upper troposphere and lower stratosphere for long-term monitoring, Atmos. Meas. Tech., 5(1),
706 17–36, doi:10.5194/amt-5-17-2012, 2012.

707 Lee, S. and Akimoto, H.: Lower tropospheric ozone trend observed in 1989–1997 at Okinawa, Japan,
708 Geophys. Res. Lett., 25(10), 1998.

709 Lefohn, A. S., Wernli, H., Shadwick, D., Limbach, S., Oltmans, S. J. and Shapiro, M.: The importance of
710 stratospheric–tropospheric transport in affecting surface ozone concentrations in the western and
711 northern tier of the United States, Atmos. Environ., 45(28), 4845–4857,
712 doi:10.1016/j.atmosenv.2011.06.014, 2011.

713 Lefohn, A. S., Wernli, H., Shadwick, D., Oltmans, S. J. and Shapiro, M.: Quantifying the importance of
714 stratospheric-tropospheric transport on surface ozone concentrations at high- and low-elevation
715 monitoring sites in the United States, Atmos. Environ., 62, 646–656,
716 doi:10.1016/j.atmosenv.2012.09.004, 2012.

717 Lelieveld, J., van Aardenne, J., Fischer, H., de Reus, M., Williams, J. and Winkler, P.: Increasing ozone
718 over the Atlantic Ocean., Science, 304(5676), 1483–7, doi:10.1126/science.1096777, 2004.

719 Levy, H., Mahlman, J. D., Moxim, W. J. and Liu, S. C.: Tropospheric ozone: The role of transport, J.
720 Geophys. Res., 90(D2), 3753, doi:10.1029/JD090iD02p03753, 1985.

721 Liang, Q., Jaeglé, L., Jaffe, D. A., Weiss-Penzias, P., Heckman, A. and Snow, J. A.: Long-range transport of
722 Asian pollution to the northeast Pacific: Seasonal variations and transport pathways of carbon
723 monoxide, J. Geophys. Res., 109(D23), n/a–n/a, doi:10.1029/2003JD004402, 2004.

724 Lin, M., Fiore, A. M., Cooper, O. R., Horowitz, L. W., Langford, A. O., Levy, H., Johnson, B. J., Naik, V.,
725 Oltmans, S. J. and Senff, C. J.: Springtime high surface ozone events over the western United States:
726 Quantifying the role of stratospheric intrusions, J. Geophys. Res., 117(D21), n/a–n/a,
727 doi:10.1029/2012JD018151, 2012a.

728 Lin, M., Fiore, A. M., Horowitz, L. W., Cooper, O. R., Naik, V., Holloway, J., Johnson, B. J., Middlebrook, A.
729 M., Oltmans, S. J., Pollack, I. B., Ryerson, T. B., Warner, J. X., Wiedinmyer, C., Wilson, J. and Wyman, B.:
730 Transport of Asian ozone pollution into surface air over the western United States in spring, J. Geophys.
731 Res., 117(4), 1–20, doi:10.1029/2011JD016961, 2012b.

732 Lin, M., Fiore, A. M., Horowitz, L. W., Langford, A. O., Oltmans, S. J., Tarasick, D. and Rieder, H. E.:
733 Climate variability modulates western US ozone air quality in spring via deep stratospheric intrusions.,
734 Nat. Commun., 6, 7105, doi:10.1038/ncomms8105, 2015.

735 Logan, J. A.: Trends in the vertical distribution of ozone: An analysis of ozonesonde data, J. Geophys.
736 Res., 99(D12), 25553, doi:10.1029/94JD02333, 1994.

737 Logan, J. A., Megretskaia, I. A., Miller, A. J., Tiao, G. C., Choi, D., Zhang, L., Stolarski, R. S., Labow, G. J.,
738 Hollandsworth, S. M., Bodeker, G. E., Claude, H., De Muer, D., Kerr, J. B., Tarasick, D. W., Oltmans, S. J.,
739 Johnson, B., Schmidlin, F., Staehelin, J., Viatte, P. and Uchino, O.: Trends in the vertical distribution of
740 ozone: A comparison of two analyses of ozonesonde data, J. Geophys. Res., 104(D21), 26373,
741 doi:10.1029/1999JD900300, 1999.

742 McDermid, I. S.: Differential absorption lidar systems for tropospheric and stratospheric ozone
743 measurements, Opt. Eng., 30(1), 22, doi:10.1117/12.55768, 1991.

744 McDermid, S., Beyerle, G., Haner, D. a and Leblanc, T.: Redesign and improved performance of the
745 tropospheric ozone lidar at the Jet Propulsion Laboratory Table Mountain Facility., Appl. Opt., 41(36),
746 7550–7555, 2002.

747 Mickley, L. J., Jacob, D. J. and Rind, D.: Uncertainty in preindustrial abundance of tropospheric ozone:
748 Implications for radiative forcing calculations, J. Geophys. Res., 106(D4), 3389,
749 doi:10.1029/2000JD900594, 2001.

750 Monks, P.: Gas-phase radical chemistry in the troposphere, Chem. Soc. Rev., 2005.

751 Naja, M. and Akimoto, H.: Contribution of regional pollution and long-range transport to the Asia-Pacific
752 region: Analysis of long-term ozonesonde data over Japan, J. Geophys. Res., 109(D21), D21306,
753 doi:10.1029/2004JD004687, 2004.

754 Naja, M., Lal, S. and Chand, D.: Diurnal and seasonal variabilities in surface ozone at a high altitude site
755 Mt Abu (24.6??N, 72.7??E, 1680 m asl) in India, Atmos. Environ., 37(30), 4205–4215, doi:10.1016/S1352-
756 2310(03)00565-X, 2003.

757 Neu, J. L., Flury, T., Manney, G. L., Santee, M. L., Livesey, N. J. and Worden, J.: Tropospheric ozone
758 variations governed by changes in stratospheric circulation, Nat. Geosci., 7(5), 340–344,
759 doi:10.1038/ngeo2138, 2014.

760 Oltmans, S. J. and Komhyr, W. D.: Surface ozone distributions and variations from 1973–1984:
761 Measurements at the NOAA Geophysical Monitoring for Climatic Change Baseline Observatories, J.
762 Geophys. Res., 91(D4), 5229, doi:10.1029/JD091iD04p05229, 1986.

763 Oltmans, S. J., Lefohn, A. S., Scheel, H. E., Harris, J. M., Levy, H., Galbally, I. E., Brunke, E.-G., Meyer, C. P.,
764 Lathrop, J. A., Johnson, B. J., Shadwick, D. S., Cuevas, E., Schmidlin, F. J., Tarasick, D. W., Claude, H., Kerr,
765 J. B., Uchino, O. and Mohnen, V.: Trends of ozone in the troposphere, Geophys. Res. Lett., 25(2), 139–
766 142, doi:10.1029/97GL03505, 1998.

767 Oltmans, S. J., Lefohn, A. S., Harris, J. M., Galbally, I., Scheel, H. E., Bodeker, G., Brunke, E., Claude, H.,
768 Tarasick, D., Johnson, B. J., Simmonds, P., Shadwick, D., Anlauf, K., Hayden, K., Schmidlin, F., Fujimoto, T.,
769 Akagi, K., Meyer, C., Nichol, S., Davies, J., Redondas, A. and Cuevas, E.: Long-term changes in
770 tropospheric ozone, Atmos. Environ., 40(17), 3156–3173, doi:10.1016/j.atmosenv.2006.01.029, 2006.

771 Oltmans, S. J., Lefohn, a. S., Shadwick, D., Harris, J. M., Scheel, H. E., Galbally, I., Tarasick, D. W.,
772 Johnson, B. J., Brunke, E. G., Claude, H., Zeng, G., Nichol, S., Schmidlin, F., Davies, J., Cuevas, E.,
773 Redondas, a., Naoe, H., Nakano, T. and Kawasato, T.: Recent tropospheric ozone changes - A pattern
774 dominated by slow or no growth, Atmos. Environ., 67, 331–351, doi:10.1016/j.atmosenv.2012.10.057,
775 2013.

776 Parrish, D. D., Millet, D. B., Goldstein, A. H. and Division, C. S.: Increasing ozone in marine boundary layer
777 in ow at the west coasts of North America and Europe, Atmos. Chem. Phys., 1303–1323,
778 doi:10.5194/acp-9-1303-2009, 2009.

779 Parrish, D. D., Law, K. S., Staehelin, J., Derwent, R., Cooper, O. R., Tanimoto, H., Volz-Thomas, A., Gilge,
780 S., Scheel, H.-E., Steinbacher, M. and Chan, E.: Long-term changes in lower tropospheric baseline ozone
781 concentrations at northern mid-latitudes, Atmos. Chem. Phys., 12(23), 11485–11504, doi:10.5194/acp-
782 12-11485-2012, 2012.

783   Petetin, H., Thouret, V., Fontaine, A., Sauvage, B., Athier, G., Blot, R., Boulanger, D., Cousin, J.-M. and
784   Nedelec, P.: Characterizing tropospheric ozone and CO around Frankfurt between 1994–2012 based on
785   MOZAIC-IAGOS aircraft measurements, Atmos. Chem. Phys. Discuss., 15(17), 23841–23891,
786   doi:10.5194/acpd-15-23841-2015, 2015.

787   Pochanart, P., Hirokawa, J. and Kajii, Y.: Influence of regional-scale anthropogenic activity in northeast
788   Asia on seasonal variations of surface ozone and carbon monoxide observed at Oki, Japan, J. Geophys.
789   Res., *104*(D3), 3621-3631, 1999.

790   Reidmiller, D. R., Fiore, A. M., Jaffe, D. A., Bergmann, D., Cuvelier, C., Dentener, F. J., Duncan, B. N.,
791   Folberth, G., Gauss, M., Gong, S., Hess, P., Jonson, J. E., Keating, T., Lupu, A., Marmer, E., Park, R.,
792   Schultz, M. G., Shindell, D. T., Szopa, S., Vivanco, M. G., Wild, O. and Zuber, A.: The influence of foreign
793   vs. North American emissions on surface ozone in the US, Atmos. Chem. Phys., 9(14), 5027–5042,
794   doi:10.5194/acp-9-5027-2009, 2009.

795   Roelofs, G.-J. and Lelieveld, J.: Model study of the influence of cross-tropopause O3 transports on
796   tropospheric O3 levels, Tellus B, 49(1), 38–55, doi:10.1034/j.1600-0889.49.issue1.3.x, 1997.

797   Simmonds, P. G., Derwent, R. G., Manning, A. L. and Spain, G.: Significant growth in surface ozone at
798   Mace   Head,   Ireland,   1987–2003,   Atmos.   Environ.,   38(28),   4769–4778,
799   doi:10.1016/j.atmosenv.2004.04.036, 2004.

800   Smit, H. G. J., Straeter, W., Johnson, B. J., Oltmans, S. J., Davies, J., Tarasick, D. W., Hoegger, B., Stubi, R.,
801   Schmidlin, F. J., Northam, T., Thompson, A. M., Witte, J. C., Boyd, I. and Posny, F.: Assessment of the
802   performance of ECC-ozonesondes under quasi-flight conditions in the environmental simulation
803   chamber: Insights from the Juelich Ozone Sonde Intercomparison Experiment (JOSIE), J. Geophys. Res.,
804   112(D19), D19306, doi:10.1029/2006JD007308, 2007.

805   Sprenger, M.: A northern hemispheric climatology of cross-tropopause exchange for the ERA15 time
806   period (1979–1993), J. Geophys. Res., 108(D12), 8521, doi:10.1029/2002JD002636, 2003.

807   Staehelin, J., Thudium, J., Buehler, R., Volz-Thomas, A. and Graber, W.: Trends in surface ozone
808   concentrations at Arosa (Switzerland), Atmos. Environ., 28(1), 75–87, doi:10.1016/1352-2310(94)90024-
809   8, 1994.

810   Stevenson, D. S., Dentener, F. J., Schultz, M. G., Ellingsen, K., van Noije, T. P. C., Wild, O., Zeng, G.,
811   Amann, M., Atherton, C. S., Bell, N., Bergmann, D. J., Bey, I., Butler, T., Cofala, J., Collins, W. J., Derwent,
812   R. G., Doherty, R. M., Drevet, J., Eskes, H. J., Fiore, A. M., Gauss, M., Hauglustaine, D. A., Horowitz, L. W.,
813   Isaksen, I. S. A., Krol, M. C., Lamarque, J.-F., Lawrence, M. G., Montanaro, V., Müller, J.-F., Pitari, G.,
814   Prather, M. J., Pyle, J. A., Rast, S., Rodriguez, J. M., Sanderson, M. G., Savage, N. H., Shindell, D. T.,
815   Strahan, S. E., Sudo, K. and Szopa, S.: Multimodel ensemble simulations of present-day and near-future
816   tropospheric ozone, J. Geophys. Res., 111(D8), D08301, doi:10.1029/2005JD006338, 2006.

817   Stohl, A.: On the pathways and timescales of intercontinental air pollution transport, J. Geophys. Res.,
818   107(D23), 4684, doi:10.1029/2001JD001396, 2002.

819   Stohl, A.: Stratosphere-troposphere exchange: A review, and what we have learned from STACCATO, J.
820   Geophys. Res., 108(D12), 8516, doi:10.1029/2002JD002490, 2003.

821   Strode, S. A., Rodriguez, J. M., Logan, J. A., Cooper, O. R., Witte, J. C., Lamsal, L. N., Damon, M., Van
822   Aartsen, B., Steenrod, S. D. and Strahan, S. E.: Trends and variability in surface ozone over the United
823   States, J. Geophys. Res., 120(17), n/a–n/a, doi:10.1002/2014JD022784, 2015.

824   Tanimoto, H., Ohara, T. and Uno, I.: Asian anthropogenic emissions and decadal trends in springtime

825 tropospheric ozone over Japan: 1998–2007, Geophys. Res. Lett., 36(23), L23802,
826 doi:10.1029/2009GL041382, 2009.

827 The Royal Society, T.: Ground-level ozone in the 21st century: future trends, impacts and policy
828 implications., 2008.

829 Thompson, A. M., Stone, J. B., Witte, J. C., Miller, S. K., Oltmans, S. J., Kucsera, T. L., Ross, K. L., Pickering,
830 K. E., Merrill, J. T., Forbes, G., Tarasick, D. W., Joseph, E., Schmidlin, F. J., McMillan, W. W., Warner, J.,
831 Hintsa, E. J. and Johnson, J. E.: Intercontinental Chemical Transport Experiment Ozonesonde Network
832 Study (IONS) 2004: 2. Tropospheric ozone budgets and variability over northeastern North America, J.
833 Geophys. Res., 112(D12), D12S13, doi:10.1029/2006JD007670, 2007.

834 Tie, X., Geng, F., Peng, L., Gao, W. and Zhao, C.: Measurement and modeling of O3 variability in
835 Shanghai, China: Application of the WRF-Chem model, Atmos. Environ., 43(28), 4289–4302,
836 doi:10.1016/j.atmosenv.2009.06.008, 2009.

837 Trickl, T., Feldmann, H., Kanter, H.-J., Scheel, H.-E., Sprenger, M., Stohl, A. and Wernli, H.: Forecasted
838 deep stratospheric intrusions over Central Europe: case studies and climatologies, Atmos. Chem. Phys.,
839 10(2), 499–524, doi:10.5194/acp-10-499-2010, 2010.

840 Trickl, T., Bärtsch-Ritter, N., Eisele, H., Furger, M., Mücke, R., Sprenger, M. and Stohl, A.: High-ozone
841 layers in the middle and upper troposphere above Central Europe: potential import from the
842 stratosphere along the subtropical jet stream, Atmos. Chem. Phys., 11(17), 9343–9366, doi:10.5194/acp-
843 11-9343-2011, 2011.

844 Tsutsumi, Y. and Matsueda, H.: Relationship of ozone and CO at the summit of Mt. Fuji (35.35°N,
845 138.73°E, 3776m above sea level) in summer 1997, Atmos. Environ., 34(4), 553–561, doi:10.1016/S1352-
846 2310(99)00238-1, 2000.

847 Vaughan, G., Price, J. D. and Howells, A.: Transport into the troposphere in a tropopause fold, Q. J. R.
848 Meteorol. Soc., 120(518), 1085–1103, doi:10.1002/qj.49712051814, 1994.

849 Volz, A. and Kley, D.: Evaluation of the Montsouris series of ozone measurements made in the
850 nineteenth century, Nature, 332(6161), 240–242, doi:10.1038/332240a0, 1988.

851 Wang, T., Ding, A., Gao, J. and Wu, W. S.: Strong ozone production in urban plumes from Beijing, China,
852 Geophys. Res. Lett., 33(21), L21806, doi:10.1029/2006GL027689, 2006.

853 WMO (World Meteorological Organization), A three-dimensional science: Second session of the
854 commission for aerology, WMO Bull., IV, 1957.

855 WMO (World Meteorological Organization), *Scientific Assessment of Ozone Depletion: 2014*, World
856 Meteorological Organization, Global Ozone Research and Monitoring Project-Report No. 55, 416 pp.,
857 Geneva, Switzerland, 2014

858 World Health Organization: Health aspects of air pollution with particulate matter, ozone and nitrogen
859 dioxide: report on a WHO working group, Bonn, Germany 13-15 January 2003., 2003.

860 Yates, E. L., Iraci, L. T., Roby, M. C., Pierce, R. B., Johnson, M. S., Reddy, P. J., Tadić, J. M., Loewenstein,
861 M. and Gore, W.: Airborne observations and modeling of springtime stratosphere-to- troposphere
862 transport over California, Atmos. Chem. Phys., 13(24), 12481–12494, doi:10.5194/acp-13-12481-2013,
863 2013.

864 Young, P. J., Archibald, A. T., Bowman, K. W., Lamarque, J.-F., Naik, V., Stevenson, D. S., Tilmes, S.,

865   Voulgarakis, A., Wild, O., Bergmann, D., Cameron-Smith, P., Cionni, I., Collins, W. J., Dalsøren, S. B.,
866   Doherty, R. M., Eyring, V., Faluvegi, G., Horowitz, L. W., Josse, B., Lee, Y. H., MacKenzie, I. A., Nagashima,
867   T., Plummer, D. A., Righi, M., Rumbold, S. T., Skeie, R. B., Shindell, D. T., Strode, S. A., Sudo, K., Szopa, S.
868   and Zeng, G.: Pre-industrial to end 21st century projections of tropospheric ozone from the Atmospheric
869   Chemistry and Climate Model Intercomparison Project (ACCMIP), Atmos. Chem. Phys., 13(4), 2063–
870   2090, doi:10.5194/acp-13-2063-2013, 2013.

871   Zbinden, R. M., Cammas, J.-P., Thouret, V., Nédélec, P., Karcher, F. and Simon, P.: Mid-latitude
872   tropospheric ozone columns from the MOZAIC program: climatology and interannual variability, Atmos.
873   Chem. Phys., 6(4), 1053–1073, doi:10.5194/acp-6-1053-2006, 2006.

874   Zhang, L., Jacob, D. J., Liu, X., Logan, J. A., Chance, K., Eldering, A. and Bojkov, B. R.: Intercomparison
875   methods for satellite measurements of atmospheric composition: application to tropospheric ozone
876   from TES and OMI, Atmos. Chem. Phys., 10(10), 4725–4739, doi:10.5194/acp-10-4725-2010, 2010.

877

878

879

880

Atmospheric
Chemistry
and Physics
Discussions

Open Access

EGU

881 **Tables:**

882

883 Table 1. Number of measurements, by month and years, performed at TMF with the tropospheric
884 ozone DIAL system. N/A indicates data not available at the time of the study

	Jan	Feb	Mar	Apr	May	Jun	Jul	Aug	Sep	Oct	Nov	Dec	Total
2000	4	2	6	4	11	12	7	10	8	1	4	2	65
2001	1	11	17	2	9	13	12	15	15	17	1	11	130
2002	6	10	6	4	0	10	11	1	6	16	6	10	93
2003	11	9	15	12	10	13	5	7	9	14	11	9	117
2004	9	8	15	14	12	6	12	13	11	10	9	8	130
2005	4	6	13	8	12	16	9	2	7	2	4	6	99
2006	11	9	6	8	14	5	2	12	12	20	11	9	106
2007	0	0	4	9	11	7	8	10	8	26	0	0	101
2008	7	11	8	13	9	4	11	10	6	11	7	11	100
2009	14	11	7	5	7	8	4	10	4	17	14	11	91
2010	0	0	3	8	0	7	4	1	4	5	0	0	44
2011	2	6	4	7	7	11	10	12	7	8	2	6	90
2012	0	9	9	1	10	13	3	2	5	8	0	9	69
2013	6	3	5	10	8	7	5	7	0	0	6	3	51
2014	9	2	5	10	13	16	15	11	15	15	14	6	131
2015	9	15	12	18	3	15	12	N/A	N/A	N/A	N/A	N/A	83
Total	93	112	135	133	136	162	130	123	117	170	103	86	1500

885

Atmospheric
Chemistry
and Physics
Discussions

886   Table 2. Ozone mixing ratio trends for the median, 5th and 95th percentiles over the period 2000-2015 as shown in Figure 6 (see text
887   for details) in ppbv·year^{-1} (%·year^{-1}). Statistically significant trends are marked in bold font

888

| | Ozone mixing ratio trends in ppbv/year (%/year) | | | | | | | | | | | | | | |
| | Year | | | Spring | | | Summer | | | Fall | | | Winter | | |
	Med.	5th P.	95th P.	Med.	5th P.	95th P.	Med.	5th P.	95th P.	Med.	5th P.	95th P.	Med.	5th P.	95th P.
17-19 km	-0.49 (-0.05)	0.25 (0.05)	-5.37 (-0.37)	-1.01 (-0.1)	3.47 (0.68)	-5.89 (-0.41)	-2.93 (-0.44)	-3.25 (-0.63)	-0.13 (-0.01)	**-8.79 (-1.39)**	**-5.80 (-1.26)**	-6.58 (-0.68)	-0.12 (-0.01)	1.37 (0.27)	-21.86 (-1.51)
12-16 km	1.56 (1.01)	-0.01 (-0.01)	2.52 (0.51)	1.10 (0.50)	0.58 (0.19)	0.29 (0.05)	0.08 (0.06)	0.20 (0.30)	0.19 (0.06)	-0.83 (-0.71)	-1.12 (-1.83)	-1.49 (-0.63)	2.54 (1.31)	0.51 (0.65)	0.95 (0.18)
7-10 km	**0.31 (0.57)**	0.01 (0.03)	**0.55 (0.54)**	**0.71 (1.10)**	0.20 (0.49)	4.31 (6.69)	**0.58 (0.98)**	0.27 (0.90)	1.01 (0.95)	-0.03 (-0.06)	-0.49 (1.62)	0.18 (0.22)	**-0.43 (-0.87)**	-0.30 (-0.91)	-1.19 (-1.41)
4-7 km	-0.14 (-0.26)	-0.33 (-0.85)	0.19 (0.17)	0.12 (0.20)	-0.29 (-0.67)	0.96 (1.17)	-0.14 (-0.24)	-0.03 (0.09)	-0.01 (-0.01)	-0.23 (0.45)	-0.82 (-2.33)	0.26 (0.06)	**-0.36 (-0.72)**	**-0.59 (-1.53)**	0.05 (0.08)

889

890

891

892

893

894

895

896

897

Atmospheric
Chemistry
and Physics
Discussions
Open Access

898 Table 3. Standard errors in ppbv·year^{-1} and p-Values associated to ozone mixing ratio trends for the median, 5th and 95th percentiles
899 included in Table 2 and shown in Figure 6. Data corresponding to statistically significant trends are marked in bold font

Ozone mixing ratio trend standard errors in ppbv/year

	Year			Spring			Summer			Fall			Winter		
	Med.	5th P.	95th P.	Med.	5th P.	95th P.	Med.	5th P.	95th P.	Med.	5th P.	95th P.	Med.	5th P.	95th P.
17-19 km	3.58	3.12	6.22	6.79	4.76	8.71	2.57	3.88	5.32	**4.47**	**2.92**	11.77	7.06	5.90	0.82
12-16 km	1.21	0.39	4.66	1.83	0.89	5.95	0.83	0.51	3.76	1.10	0.85	3.84	2.54	1.16	10.05
7-10 km	**0.15**	0.19	**0.30**	**0.25**	0.38	3.32	**0.28**	0.20	1.20	0.25	0.35	0.97	**0.18**	0.27	1.00
4-7 km	0.14	0.24	0.25	0.31	0.36	0.56	0.21	0.35	0.38	0.31	0.38	0.53	**0.16**	**0.18**	0.28

900

p-Values

	Year			Spring			Summer			Fall			Winter		
	Med.	5th P.	95th P.	Med.	5th P.	95th P.	Med.	5th P.	95th P.	Med.	5th P.	95th P.	Med.	5th P.	95th
17-19 km	0.89	0.94	0.40	0.88	0.48	0.51	0.27	0.41	0.98	**0.07**	**0.07**	0.60	0.99	0.82	0.17
12-16 km	0.22	0.98	0.60	0.55	0.52	0.96	0.92	0.71	0.96	0.47	0.21	0.70	0.29	0.67	0.92
7-10 km	**0.06**	0.94	0.09	**0.01**	0.60	0.22	**0.05**	0.19	0.41	0.91	0.18	0.86	**0.03**	0.28	0.25
4-7 km	0.33	0.19	0.44	0.70	0.44	0.11	0.52	0.92	0.98	0.47	0.05	0.63	**0.04**	**4.10^{-3}**	0.85

Table 4. Number of air parcels ending at TMF during lidar measurements over the period 2000-2015, classified as "Stratosphere", "Central America, "ABL","AFT" and "Pacific Ocean" (see text for details)

	Strat	Cent. Am	ABL	AFT	Pac
14 km	1150 (78%)	47 (3%)	0 (0%)	5 (0%)	270 (18%)
13 km	853 (58%)	69 (5%)	1 (0%)	20 (1%)	519 (35%)
12 km	515 (35%)	86 (6%)	4 (0%)	61 (4%)	798 (54%)
11 km	321 (22%)	89 (6%)	16 (1%)	51 (3%)	985 (67%)
10 km	199 (13%)	94 (6%)	17 (1%)	93 (6%)	1058 (71%)
9 km	118 (8%)	98 (7%)	18 (1%)	92 (6%)	1146 (77%)
8 km	70 (5%)	103 (7%)	19 (1%)	82 (6%)	1197 (91%)
7 km	62 (4%)	110 (7%)	19 (1%)	84 (6%)	1194 (81%)
6 km	24 (2%)	133 (9%)	11 (1%)	67 (5%)	1226 (83%)
5 km	31 (2%)	161 (11%)	12 (1%)	87 (6%)	1169 (79%)

Atmospheric
Chemistry
and Physics
Discussions

Open Access
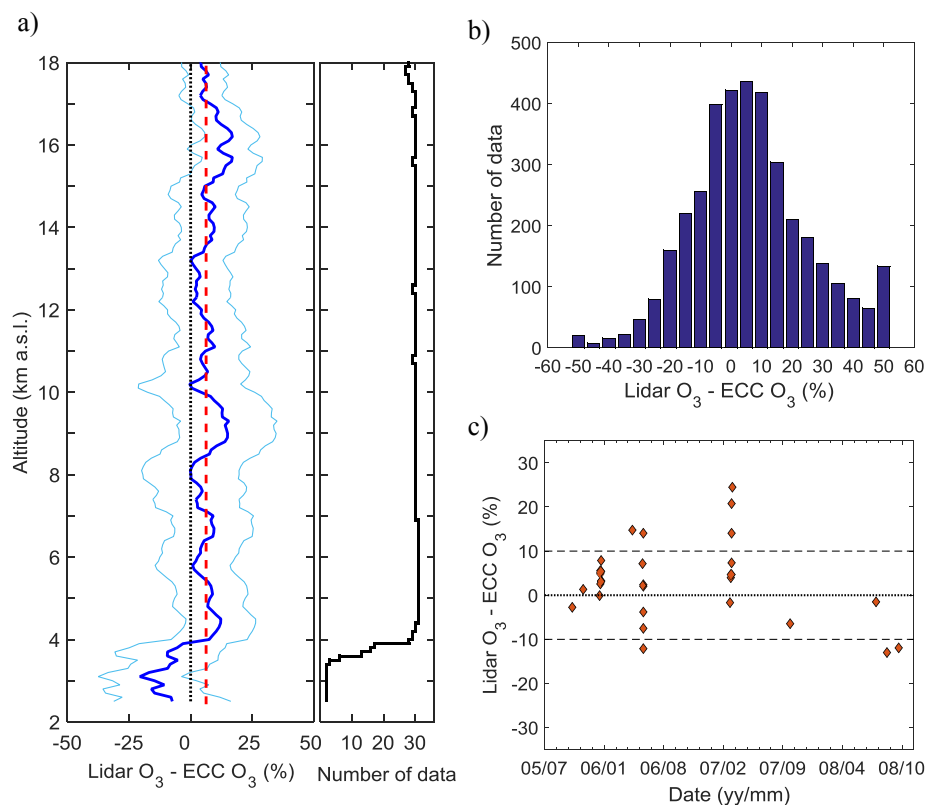
Figure 1. a) Profile of the mean relative difference between the lidar and the ECC ozone number density for the 32 simultaneous measurements (dark blue). Lidar uncertainty (light blue) and mean relative difference obtained between 4 and 16 km (red dotted line) are superimposed. The black solid curve shows the number of data points at each altitude. b) Histogram of the difference between the lidar and the ECC ozone number density. c) Column-averaged (below 8 km) difference between the lidar and the ECC sonde for each coincidence
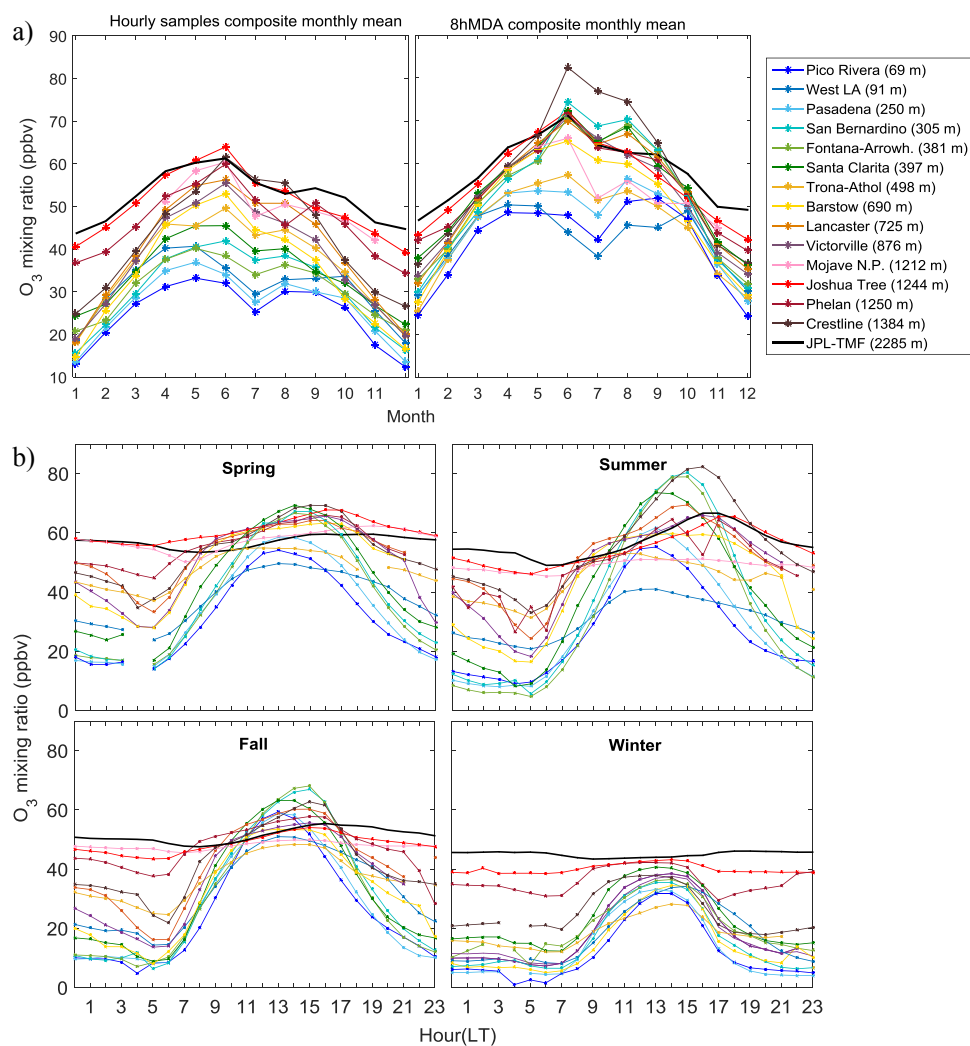
Figure 2. a) Composite monthly mean surface ozone at TMF and nearby ARB stations obtained from hourly samples (left) and 8hMDA values (right) for the period 2013-2015. b) Composite mean ozone daily cycle at TMF and nearby ARB stations for the four seasons for the period 2013-2015
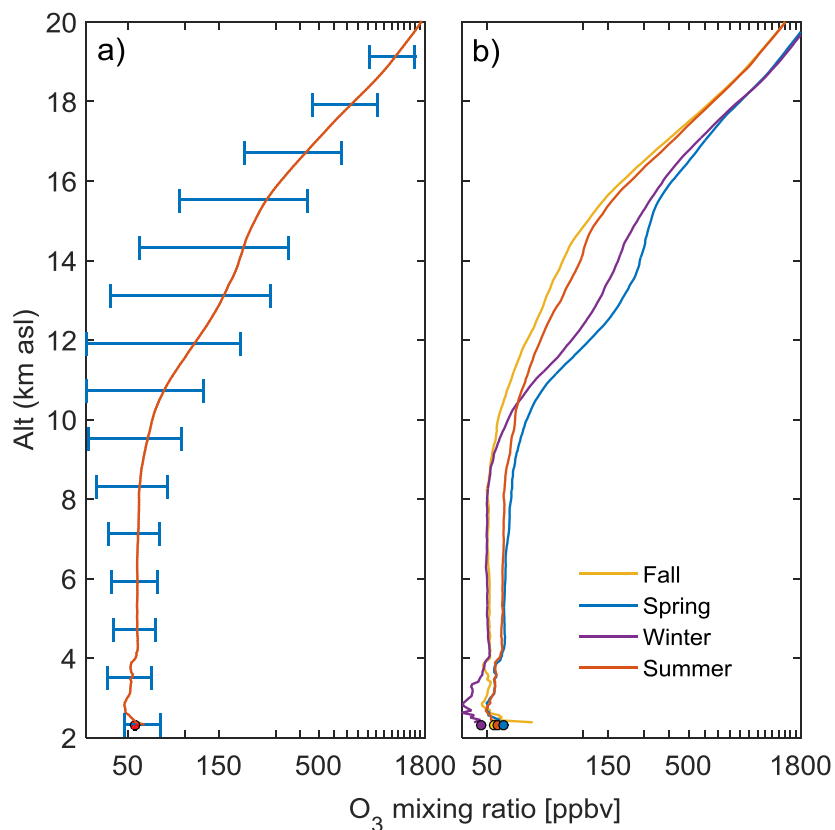
Figure 3. a) Ozone mixing ratio climatological average (2000-2015) computed from the TMF lidar measurements (red curve). The cyan horizontal bars indicate the standard deviation at intervals of 1-km. The red dot at the bottom indicates the mean surface ozone mixing ratio (2013-2015) measured simultaneously with lidar. b) Seasonally-averaged ozone mixing ratio profiles for spring (MAM), summer (JJA), fall (SON) and winter (DJF). The dots at the bottom indicate the corresponding surface ozone seasonal averages

Atmospheric
Chemistry
and Physics
Discussions

Open Access
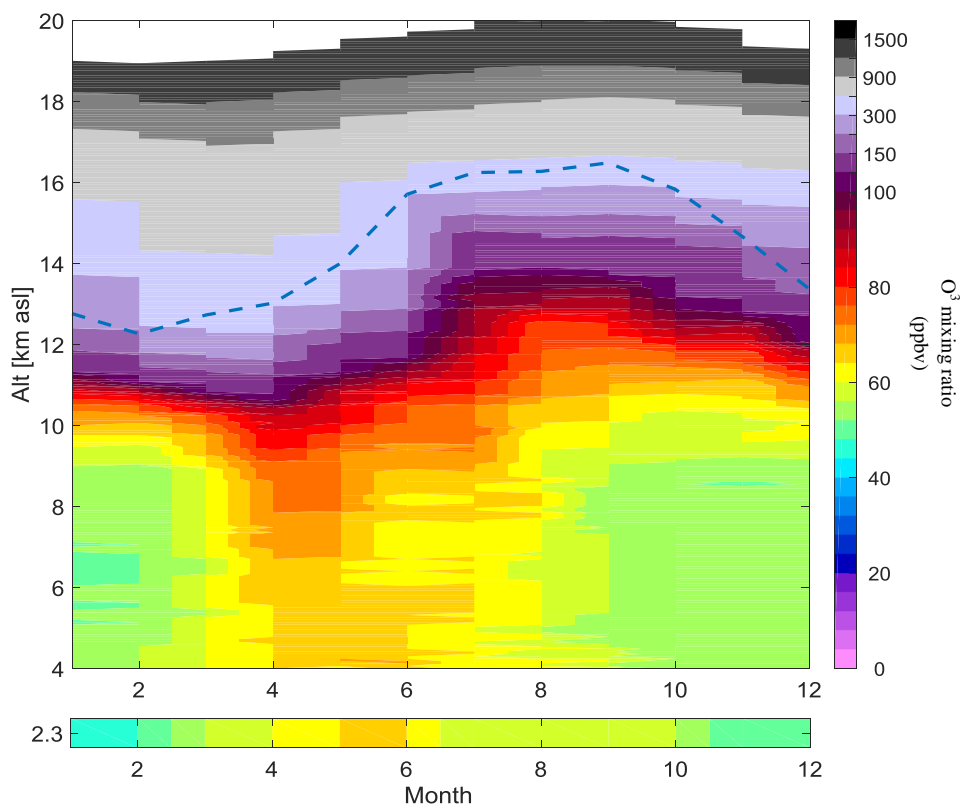
Figure 4. Composite monthly mean ozone mixing ratio (2000-2015) computed from the TMF lidar measurements. The dashed line indicates the climatological tropopause above the site (WMO definition). Bottom strip: Composite monthly mean ozone mixing ratio (2000-2015) from the surface measurements
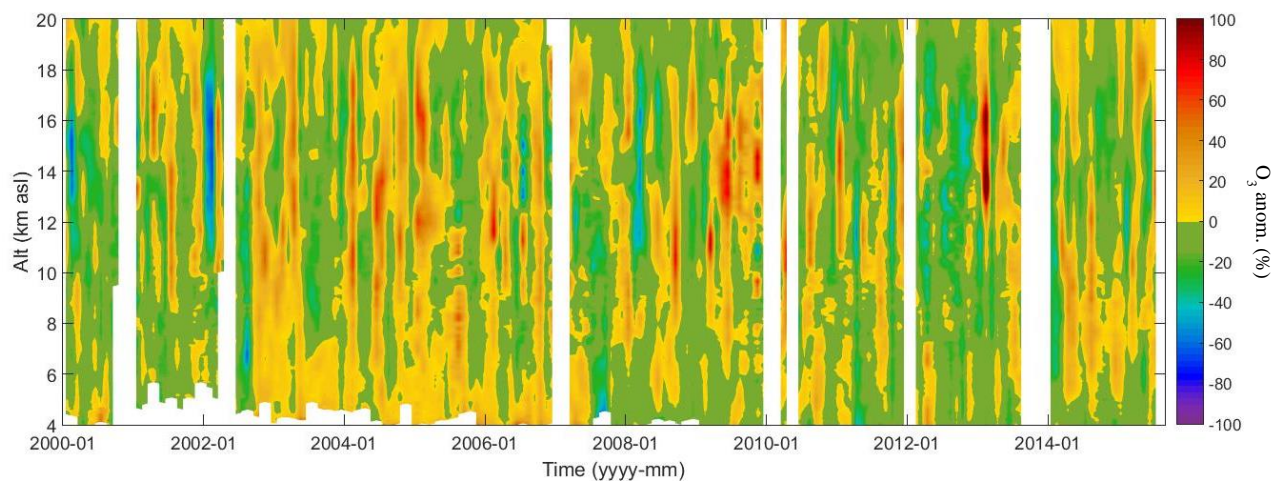
Figure 5. Deseasonalized ozone mixing ratio above TMF. Anomalies (in %) were computed with respect to the climatological (2000-2015) monthly mean
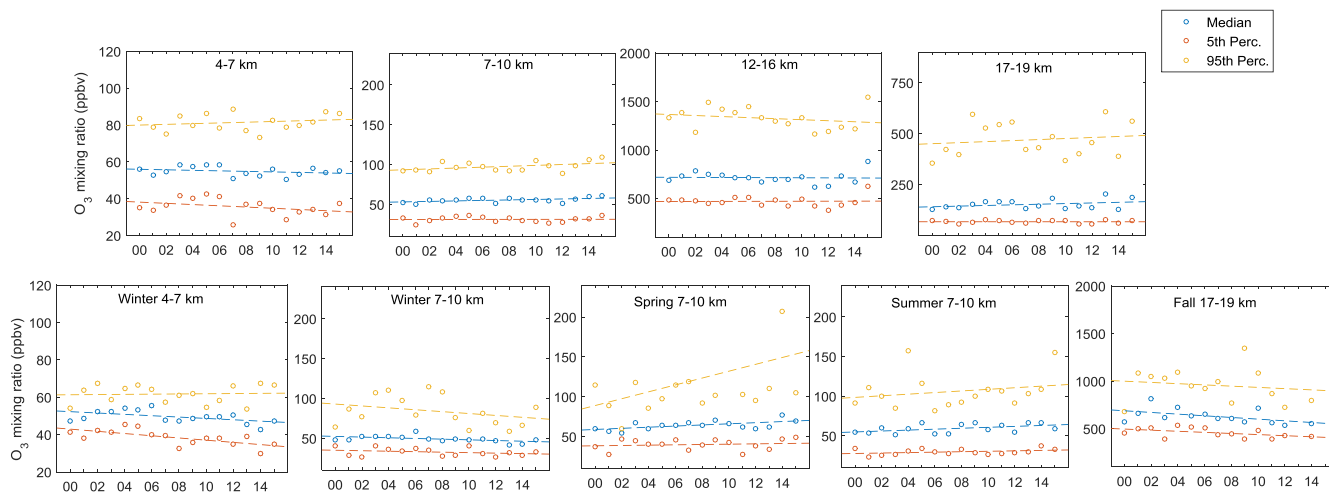
Figure 6. Time series of the median (blue), 5th (orange) and 95th (yellow) percentile ozone values at different altitude layers for the full year (top) and for selected seasons and altitude layers (bottom) obtained from the TMF lidar measurements. Dashed lines represent the linear fit for each time series
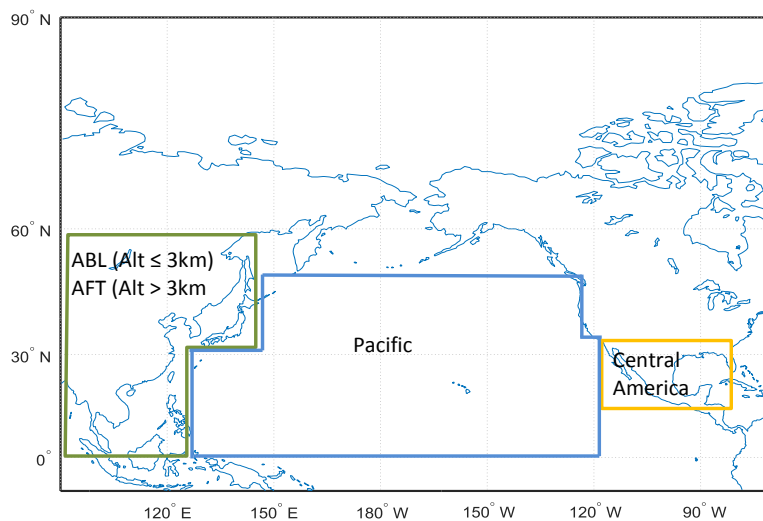
Figure 7. Geographical boundaries used to characterize the air parcels associated with the 8-day backward trajectories ending at TMF during the lidar measurements over the period 2000-2015
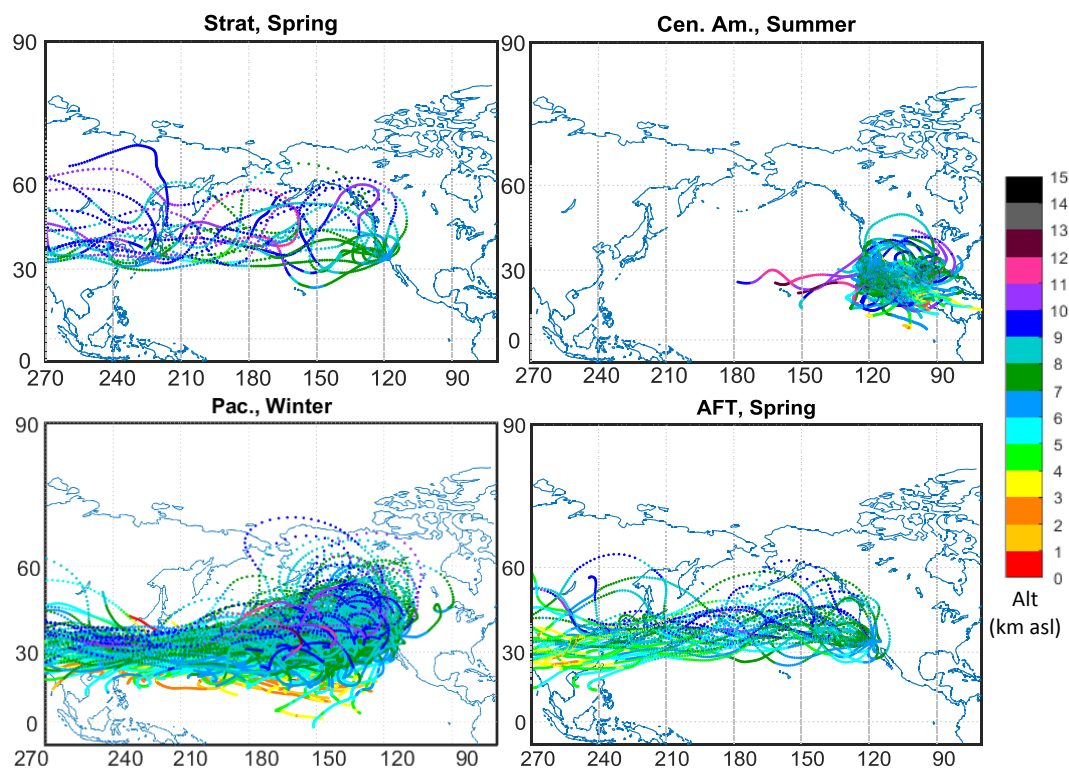
Figure 8. Examples of HYSPLIT 8-day backward trajectories arriving at TMF at 7 km altitude for four selected seasons and categories (see text for details)
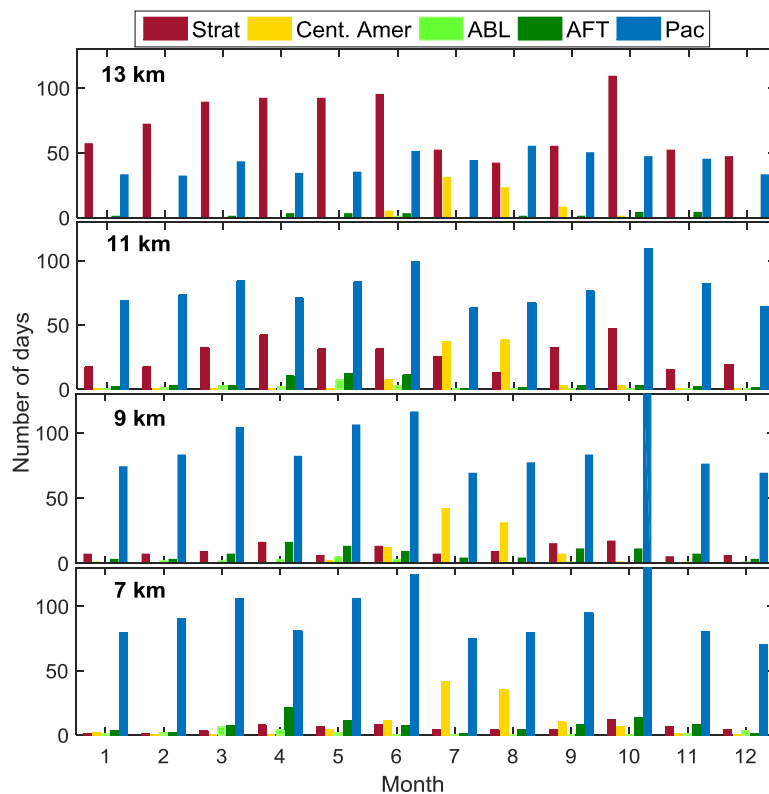
Figure 9. Distribution of the five categories identified for each trajectory ending at TMF during the lidar measurements over the period 2000-2015. The number of occurrences is given for each month of the year, and for four different altitude layers

Atmospheric
Chemistry
and Physics
Discussions

Open Access
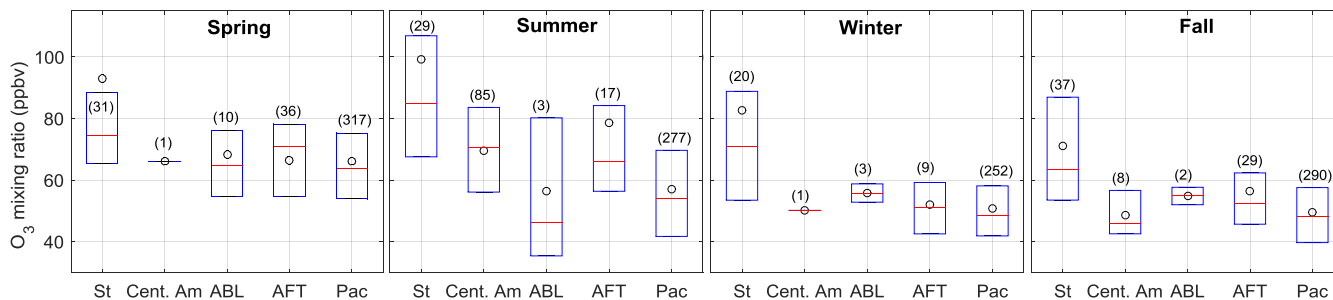
Figure 10. Box plot of the ozone mixing ratios measured within the air masses arriving at TMF at 9 km for the five identified categories (see text for details) and the four seasons. The black dot represents the mean value, the red line is the median and the box limits correspond to the 25th and 75th percentiles. The numbers between parentheses indicate the number of associated trajectories
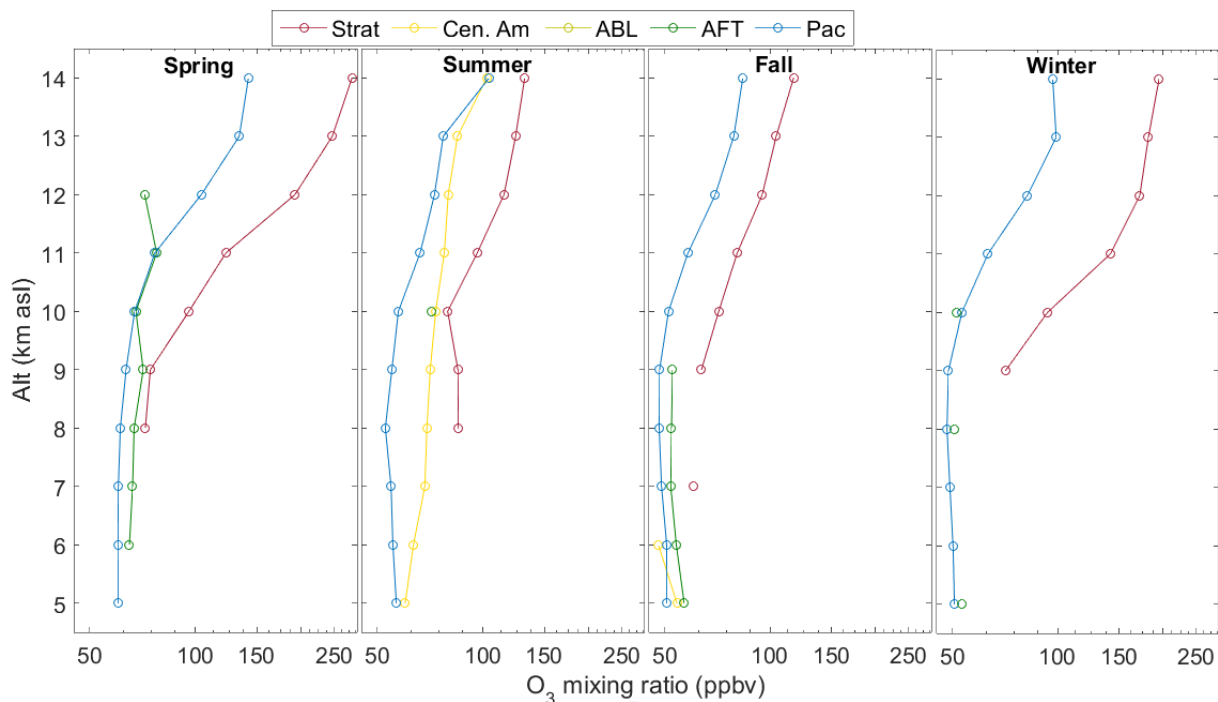
Figure 11. Composite profiles of the ozone mixing ratio associated with the different categories and for each season. Results are shown only when the number of samples for a given category was larger than 5% of the total number of samples in that season
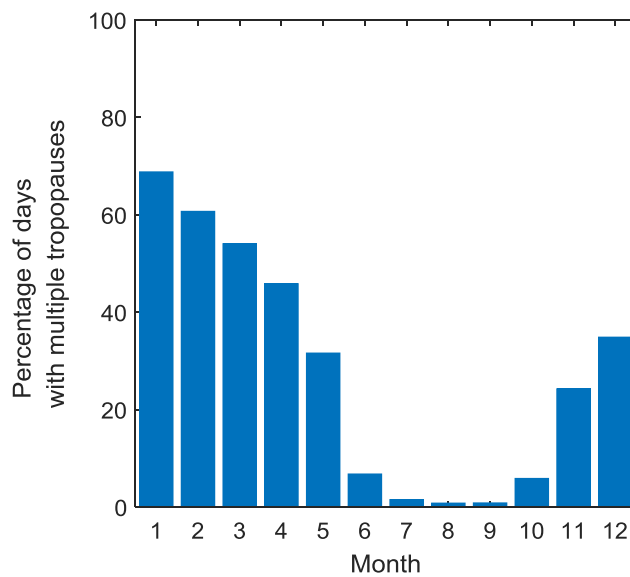
Figure 12. Monthly distribution of occurrences (in %) of double tropopauses above TMF. The number of days with tropopause folds is normalized to the total number of measurements per month compiled in Table1

Atmospheric
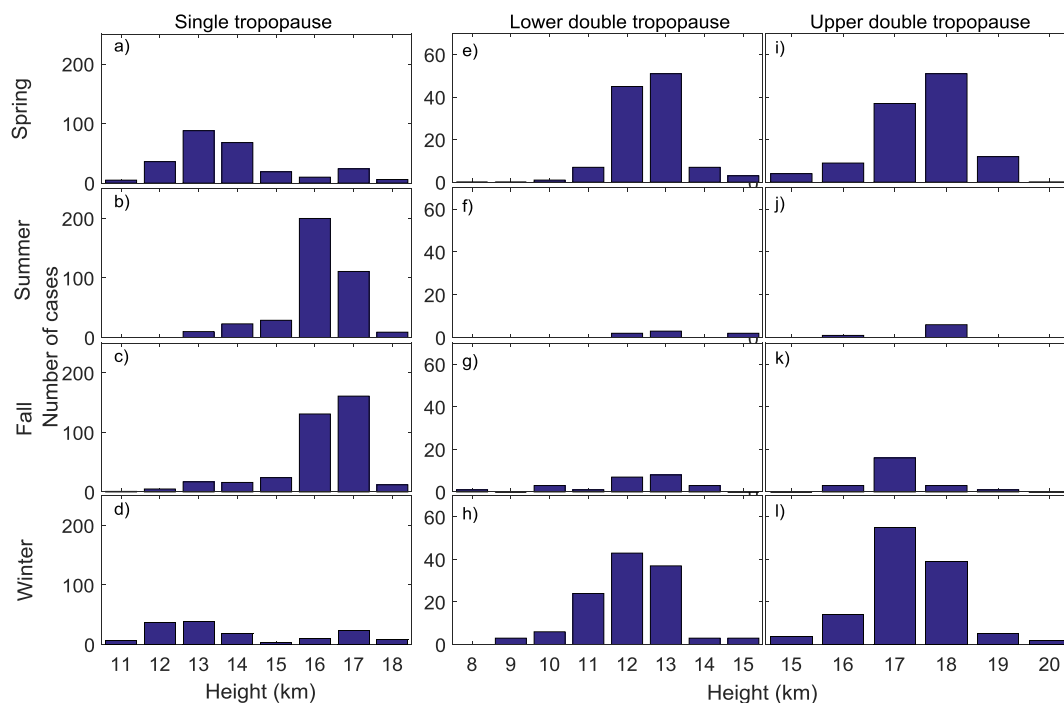Chemistry
and Physics
Discussions

Figure 13. a) to d) Altitude distribution of the tropopause above TMF for spring, summer, fall and winter respectively, and in the absence of double-tropopause. e) to h) Altitude distribution of the lower (first) tropopause above TMF for spring, summer, fall and winter respectively, and in the presence of a double-tropopause. i) to l) Same as e) to h) but for the upper or second tropopause. All computations were made at the times of the TMF lidar measurements
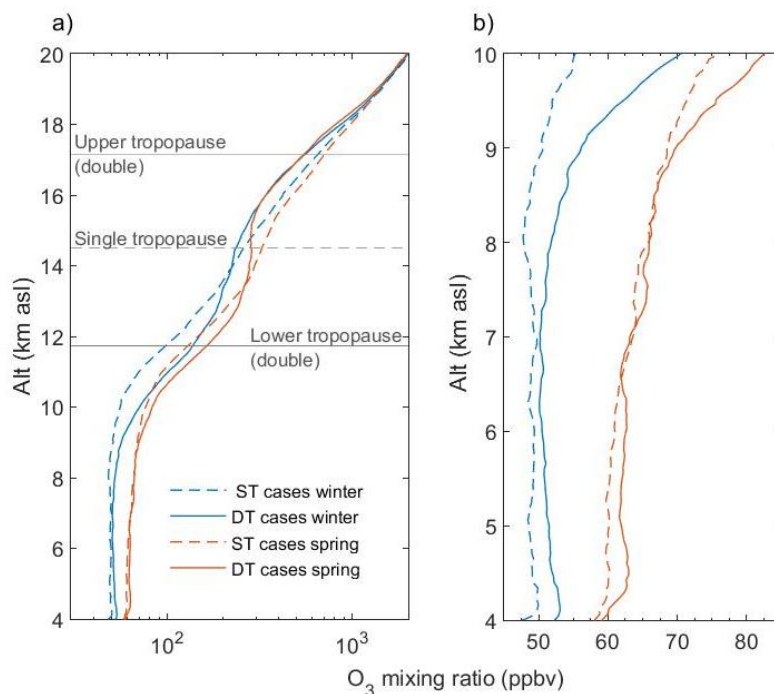
Figure 14. Winter- (cyan) and Spring- (red) averaged ozone mixing ratio profiles computed in the presence of a double tropopause (DT, solid curves) and single tropopause (ST, dashed curves). The horizontal solid grey curves depict the average altitude of the lower and upper tropopauses when a double tropopause was identified. The horizontal dashed grey line corresponds to the average altitude of the tropopause when a single tropopause was identified. b) Same as a) but zoomed on the tropospheric part of the profiles (4-10 km)